Theor Chem Acc (2011) 128:91–113
DOI 10.1007/s00214-010-0767-x

REGULAR ARTICLE

Hydrogenated amorphous silicon nanostructures: novel structure–reactivity relationships for cyclization and ring opening in the gas phase

Andrew J. Adamczyk · Marie-Francoise Reyniers · Guy B. Marin · Linda J. Broadbelt

Received: 15 April 2010 / Accepted: 7 May 2010 / Published online: 30 May 2010

Abstract The effects of the reactive center connectivity and internal rotations on the reactivity of hydrogenated silicon nanostructures toward cyclization and ring opening pathways have been investigated. Rate coefficients for 25 cyclization and ring opening reactions for hydrides containing up to eight silicon atoms have been calculated using G3//B3LYP. The overall reactions exhibit two elementary steps. Overcoming the first barrier results in the formation of a hydrogen-bridged cyclic intermediate from a substituted silylene. Passing over the second barrier converts this intermediate into a cyclic silicon hydride. The rate-determining step varied according to the ring size formed and the temperature. Assuming a rate-determining step, values for the single-event Arrhenius pre-exponential factor, $\tilde{A}$, and the activation energy, E_a, were calculated from G3//B3LYP rate coefficients corrected for internal rotations, and a group additivity scheme was developed to predict $\tilde{A}$ and E_a. The values predicted by group additivity are more accurate than structure–reactivity relationships currently used in the literature, which rely on a representative $\tilde{A}$ value for each reaction class and the Evans-Polanyi correlation to predict E_a. Internal rotation corrections played a prominent role in cyclization pathways, impacting $\tilde{A}$ values for larger ring formation reactions more strongly than any variations in the connectivity of the reactive center.

Keywords Isomerization · Non-linear Arrhenius plots · Pyrolysis · Reactive intermediate · Ring statistics · Silicon hydride

1 Introduction

Hydrogenated silicon nanostructures containing small- to medium-sized rings are of key interest due to formation in the gas phase during the pyrolytic deposition of polycrystalline silicon [1, 2]. Under chemical vapor deposition conditions to produce semiconductor grade polycrystalline silicon, saturated silicon hydrides in the gas phase eliminate dihydrogen and isomerize to form clusters with increased polycyclic nature. These clusters deposit onto the growing silicon wafer to create point defects [3]. Alternatively, polycyclic silicon clusters of diameter less than 10 nm have attracted positive attention due to size- and surface-dependent photoluminescent properties which can be tailored for new materials development [4] and biological applications [5]. Moreover, cyclization and ring opening reactions of larger ring sizes are important for low-temperature applications such as polysilane polymers [6, 7] and solution-processed electronics [8, 9]. A detailed microkinetic understanding of the early growth stages of polycyclic silicon hydrides is needed to predict cluster diameter, crystallinity, and surface characteristics under different operating conditions.

The formation of cyclic and polycyclic structures is a route by which silicon hydrides can dehydrogenate and further stabilize divalent centers by intramolecular polymerization (Fig. 1) [10]. Absolute rate measurements of

Electronic supplementary material The online version of this article (doi:10.1007/s00214-010-0767-x) contains supplementary material, which is available to authorized users.

A. J. Adamczyk · L. J. Broadbelt (✉)
Department of Chemical and Biological Engineering, Northwestern University, Evanston, IL 60208-3120, USA
e-mail: broadbelt@northwestern.edu

M.-F. Reyniers · G. B. Marin
Laboratory for Chemical Technology, Ghent University, 9000 Ghent, Belgium

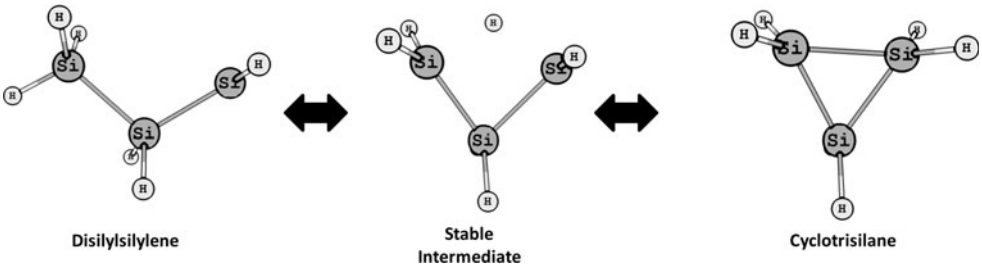

Fig. 1 Reference reaction for cyclization/ring opening through Si–H bond insertion

silicon hydride cyclization and ring opening reactions are not available (i.e., for species containing a backbone of Si–Si σ bonds and only hydrogen substituents). Controlled silicon hydride syntheses have been achieved with cyclopentasilane [11] and cyclohexasilane [12]. Only heavily substituted derivatives of smaller cyclic species comprised a backbone of Si–Si σ bonds have been synthesized: (1) four-membered ring in 1921 by Kipping et al. [13], (2) three-membered ring in 1982 by Masamune et al. [14] and (3) a polycyclic species in 1972 by West and Indriksons [15]. Others have since studied and confirmed the importance of cyclization and ring opening pathways experimentally [16–21] for heavily substituted systems and theoretically [22–41] for the analyses of structure and energetics of cyclic and polycyclic silicon hydrides. Extensive theoretical investigations [42–45] have also been performed on the thermochemistry of acyclic and cyclic silicon hydrides and, in certain cases, the effects of anharmonic vibrations on thermochemistry. Interest in cyclic silicon hydrides extends beyond a backbone of Si–Si σ bonds to heterocyclic species containing additional elements including carbon [46–52], oxygen [53, 54] and nitrogen [55, 56] atoms. Nonetheless, detailed exploration of the cyclization and ring opening reaction kinetics of silicon hydrides containing small- to medium-sized rings has never been undertaken to our knowledge, and it is precisely this information that is necessary to describe hydrogenated amorphous silicon nanostructure growth kinetics.

Recently, automated network generation techniques [57–63] have emerged that allow the kinetics of silicon cluster formation to be described at the mechanistic level [2]. Rate coefficients must be estimated for every elementary step comprising the mechanistic model, and kinetic correlations are used to make this tractable. One common method for predicting E_a is the Evans–Polanyi [64] correlation depicted in Eq. 1, where E_o and γ are parameters that are determined from linear regression against experimental or theoretical values and are constant for a given reaction class. For cyclization and ring opening reactions, Evans–Polanyi parameters of $E_o = 0$ kcal mol^{-1}, $\gamma = 0$ (cyclization), and $\gamma = 1$ (ring opening) [2, 65], and a representative single-event value of $\tilde{A}_{\text{ring opening}} = 2 \times 10^{15}\,\text{s}^{-1}$ [1, 66] have been used. However, it has not been demonstrated that these literature values are accurate for cyclization and ring opening reactions, as the kinetic correlations in the literature have been generalized from silylene addition and elimination reactions.

$$E_a = E_o + \gamma\,\Delta H_{\text{Rxn}}. \tag{1}$$

An alternative approach for estimating kinetic parameters is transition state group additivity (TSGA). Inspired by the pioneering group additivity methods developed by Benson [67] for thermochemical property estimation, which have been successfully applied over a wide range of temperatures to silicon hydrides for S, C_p and ΔH_f estimation by Wong et al. [45], Sumathi et al. [68–70] first applied group additivity to the thermodynamic properties of the transition state for rate coefficient prediction of hydrogen abstraction reactions. Saeys et al. [71, 72] and Sabbe et al. [73] then improved the method for reaction classes governing hydrocarbon chemistry by allowing group additivity to calculate the *differences* in properties between the transition state and the reactant(s). The basic method treats reactions for which predictions of kinetic parameters are desired as perturbations to a reference reaction. This approach builds on the work by Willems and Froment [74, 75] who predicted pre-exponential factors and activation energies based on structural deviations of the reactant(s) from a reference reaction using a combination of transition state theory (TST), statistical thermodynamics and group additivity for thermodynamic properties to describe the steam cracking of hydrocarbons. However, no quantum chemical calculations were used to explicitly calculate $\tilde{A}$ and E_a for individual reactions. Saeys et al. [71, 72] extended their approach to the prediction of activation energies for hydrogen abstraction and radical addition/β-scission reactions based on explicit transition state geometries calculated using quantum chemistry (CBS-QB3). Sabbe et al. [73] then extended the TSGA method to the prediction of pre-exponential factors for radical addition/β-scission reactions using CBS-QB3 as well. Truong et al. [76, 77] adopted a similar approach for predicting rate coefficients of hydrogen abstraction reactions that they termed reaction class TST, which relies on a reference

reaction, the reaction energy and the differential barrier height.

The TSGA method possesses several advantages that should interest kineticists seeking parameters for cyclization and ring opening reactions in silicon hydrides. This method requires a number of parameters similar to that of the Evans–Polanyi correlation, but (1) allows one to gain insight into the effects of structural changes on the reactive center during reaction, (2) implements multiple values of $\tilde{A}$ for each reaction class, and (3) circumvents the need to calculate accurate standard enthalpies and Gibbs free energies of reaction as required for the Evans–Polanyi correlation and subsequent calculation of the reverse rate coefficient, respectively. The knowledge of the number and the type of substituents on the reactive center for a given reaction class is sufficient to allow accurate kinetic parameter estimation.

This paper presents an extension of the TSGA approach to silicon hydride chemistry and specifically examines the cyclization and ring opening reactions for molecules containing up to eight silicon atoms. All elementary steps studied involved monofunctional compounds, i.e., molecules containing one divalent center. Species containing rings with three to six silicon atoms were considered. The composite method of G3//B3LYP [78] was used to calculate the electronic energy, and then statistical thermodynamics was applied to all reactants and transition states to incorporate temperature effects. Single-event rate coefficients at 1 atm and 298–1,500 K were calculated using TST, corrected for internal rotations [42, 79–86], and then activation energies, E_a, and single-event pre-exponential factors, $\tilde{A}$, were regressed. A training set of E_a and $\tilde{A}$ values was used to regress TSGA values. These group additivity parameters were then validated against reactions not used in the training set. Lastly, a comparison of the rate coefficients predicted by the current literature methods and those calculated using G3//B3LYP and TSGA was performed.

2 Computational methodology

2.1 Quantum chemical calculations, TST, and statistical thermodynamics

Quantum chemical calculations were performed with *Gaussian 03* [87] for all the reactions summarized in Fig. 2 (training set) and Fig. 3 (validation set). All electronic energies for substituted silylenes, cyclic silanes, transition states and intermediates were calculated using the G3//B3LYP method [78], which uses B3LYP geometries and higher-level corrections based on single point energies. For all results reported, the electronic wavefunctions for all substituted silylenes, cyclic silanes, transition states and reactive intermediates were optimized in the lowest energy singlet state [88, 89]. Geometries and harmonic frequencies of the lowest energy conformers were determined at the B3LYP/6-31G(d) level. The harmonic frequencies and zero point energy (ZPE) were scaled by factors of 0.96 and 0.98, respectively, to account for anharmonicity in the normal

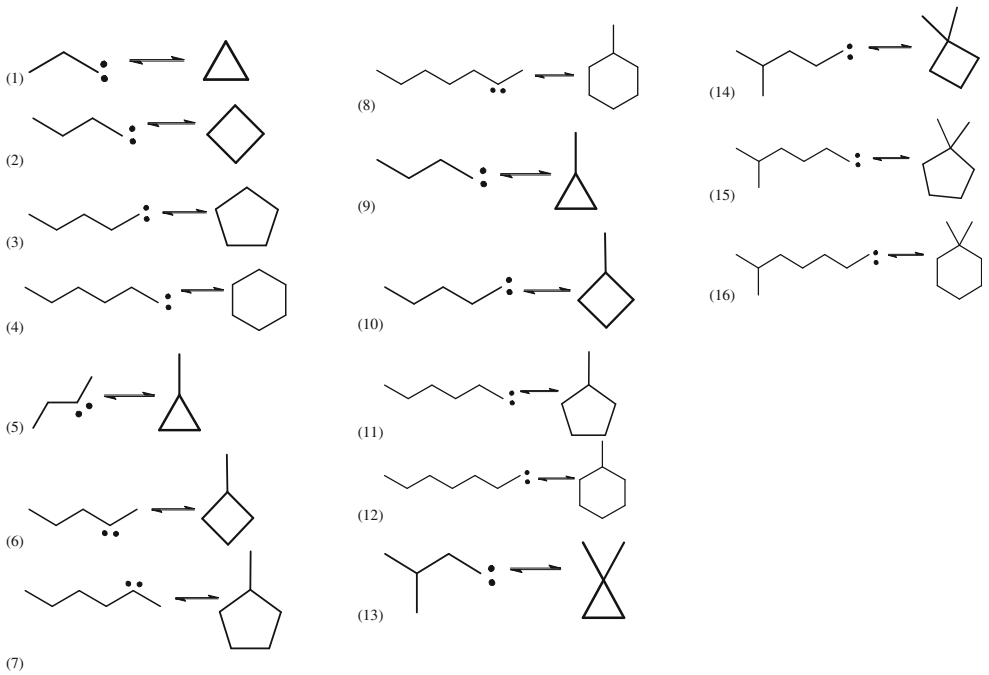

Fig. 2 Training set reactions

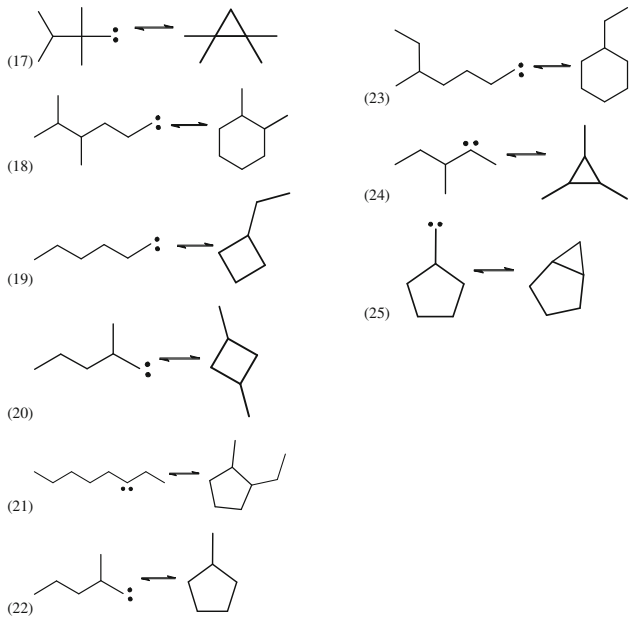

Fig. 3 Validation set reactions

vibrational modes as suggested by Scott and Radom [90]. The Cartesian coordinates and unscaled frequencies for all substituted silylenes, cyclic silanes and only the transition states of the rate-determining step (i.e., the second step in the cyclization direction for three-membered ring formation reactions and the first step in the cyclization direction for four-, five-, and six-membered ring formation reactions) can be found in the Supporting Information.

Using conventional statistical thermodynamics, partition functions based on the harmonic oscillator and rigid rotor approximations were used to calculate thermodynamic and kinetic properties as a function of temperature. Internal rotations in the substituted silylenes that were more appropriately treated as free rotors that do not cancel between the reactant and the transition state were quantified using one-dimensional free rotor approximations. The potential energy barriers to rotation of the non-canceling torsional modes in the substituted silylenes are sufficiently low to assume free rotations under pyrolytic conditions (see "Results and discussion"). This procedure was performed automatically using the *CalcK* script developed by our group [82]. Anharmonic small ring movements (e.g., the pseudorotation of cyclopentasilanes and the ring puckering of cyclotetrasilanes) were not treated [42, 91].

To benchmark the G3//B3LYP method used in this theoretical study, Weizmann-1 (W-1) calculations [92] were performed and found to be in excellent agreement with the G3//B3LYP results. Assuming the second step in the cyclization direction is the rate-determining step for three-membered ring formation and correcting for internal rotations (see "Results and discussion"), values for Arrhenius parameters predicted with G3//B3LYP and W-1 methods are provided in Table 1. Comparison of W-1 rate coefficients to G3//B3LYP values for the cyclization and ring opening reactions at 1,000 K are provided in Table 1. In addition, G3//B3LYP was a reasonable choice because the TSGA database is intended to be used in conjunction with an existing G3//B3LYP database developed by our group for the estimation of silicon hydride thermochemical properties [45].

The rate-determining step and thus the relevant transition state vary as a function of the ring size being formed and the temperature (see "Results and discussion"). Transition states for the rate-determining step of three-membered ring formation reactions were found using the potential energy surface interpolation method QST3. The imaginary frequency of each transition state was animated and intrinsic reaction coordinate following was carried out to confirm that the normal vibrational mode pertained to the reaction coordinate of interest. Conventional TST [93] was then used to calculate rate coefficients according to the macroscopic formulation in Eq. 2 at 1 atm assuming an ideal gas:

Table 1 G3//B3LYP and Weizmann-1 (W-1) Arrhenius parameters, zero point energy corrected barriers, and enthalpy of reaction for reaction 1 at 298 K and 1 atm corrected for internal rotations

Level of theory	Cyclization				Ring opening		
	E_o (kcal mol^{-1})	Log $\tilde{A}$	E_a (kcal mol^{-1})	ΔH^{298}_{Rxn} (kcal mol^{-1})	E_o (kcal mol^{-1})	Log $\tilde{A}$	E_a (kcal mol^{-1})
G3//B3LYP	−0.8	12.5	−1.0	−18.1	16.8	13.1	17.2
Weizmann-1	−1.3	12.5	−1.5	−19.3	17.5	13.1	17.9

Reaction 1	$k^{G3//B3LYP}/k^{W-1}$
Comparison of *W*-1 rate coefficients at 1,000 K and 1 atm for reaction 1 to the G3//B3LYP values calculated in this study	
$SiHSiH_2SiH_3 \rightarrow$ cyclo-Si_3H_6	0.64
cyclo-$Si_3H_6 \rightarrow SiHSiH_2SiH_3$	1.40

The kinetic parameters were calculated assuming that the first step in the cyclization direction is equilibrated. $\tilde{A}$ has units of s^{-1}

$$k^{\mathrm{TST}}(T) = n_{\mathrm{d}}\tilde{k}(T) = n_{\mathrm{d}}\Lambda \exp\left(\frac{\Delta S^{\neq}}{R}\right)\exp\left(\frac{-\Delta H^{\neq}}{\mathrm{RT}}\right), \quad (2)$$

where Λ is defined in Eq. 3:

$$\Lambda = \kappa(T)\frac{k_{\mathrm{B}}T\left(V_{\mathrm{m}}^{\mathrm{o}}\right)^{-\Delta n}}{h} \quad (3)$$

where $\tilde{k}$ is the single-event rate coefficient; $\kappa(T)$ is the Wigner tunneling correction [94] at temperature T; k_{B} is Boltzmann's constant; h is Planck's constant; $V_{\mathrm{m}}^{\mathrm{o}}$ is the standard molar volume; R is the ideal gas constant; $\Delta S^{\neq}$ is the standard entropy of activation; $\Delta H^{\neq}$ is the standard enthalpy of activation; Δn is the change in the number of moles going from the reactant to the transition state (i.e., zero in both directions for isomerization); and n_{d} is the reaction path degeneracy, or number of single events [95]. $\Delta H^{\neq}$ and $\Delta S^{\neq}$ are calculated using standard formulae [93].

Calculating rate coefficients for the rate-determining step of four-, five- and six-membered ring formation reactions required a variational search of the reaction coordinate for the point of minimum flux constituting the dynamic bottleneck to the reaction using geometric constraints (i.e., one-dimensional search in coordinate space) [96, 97]. The calculation of rate coefficients at the point of maximum standard Gibbs free energy of activation was performed assuming a local equilibrium between the generalized (or variational) transition state (GT) and the reactant. The generalized transition state along the reaction coordinate was chosen to satisfy Eq. 4 to minimize the rate coefficient.

$$k^{\mathrm{VTST}}(T) = n_{\mathrm{d}}\tilde{k}^{\mathrm{VTST}}(T) = n_{\mathrm{d}}\min_{s}\left[\Lambda \exp\left(\frac{-\Delta G^{\mathrm{GT}}(T,s)}{\mathrm{RT}}\right)\right] \quad (4)$$

where $\tilde{k}^{\mathrm{VTST}}$ is the single-event rate coefficient from one-dimensional variational TST; n_{d} is defined in Eq. 2; Λ is defined in Eq. 3; ΔG^{GT} is the standard Gibbs free energy of activation; s is the reaction coordinate of interest leading from the reactant (negative s) to the product (positive s).

The single-event parameters of the Arrhenius relationship, $\tilde{A}$ and E_{a}, were obtained by fitting ln $\tilde{k}$ versus T^{-1} over the temperature range of 298–1,500 K. This procedure was performed automatically using the *CalcK* script developed by our group [82]. Arrhenius behavior was obeyed well; for example, reactions 1 through 4 had linear regression coefficients equal to 1 for the ring opening pathway. Cyclization pathways had linear regression coefficients equal to 0.997, 0.997, 0.981 and 0.965 for reactions 1 through 4, respectively, as the Arrhenius fit was more non-linear for larger ring formation reactions.

2.2 TSGA model and application to cyclization and ring opening reactions

TSGA was adapted to describe E_{a} and $\tilde{A}$ of the cyclization and ring opening reaction for each single event as shown in Eqs. 5, 6, and 7 according to the labeling in Fig. 4. E_{a} and $\tilde{A}$ are calculated based on deviations from a reference reaction. The deviations are categorized as those due to the two silicon atoms central to the reaction, and primary (X, Y) and secondary (N, M) contributions, where secondary contributions are grouped together as next-nearest neighbors (*NNN*).

$$E_{\mathrm{a}} = E_{\mathrm{a}}^{\mathrm{Ref}} + \sum_{i=1}^{2}\Delta\mathrm{GAV}_{E_{\mathrm{a}}}^{0}(\mathrm{Si}_i) + \Delta\mathrm{GAV}_{E_{\mathrm{a}}}^{0}(X_1) + \sum_{i=1}^{2}\Delta\mathrm{GAV}_{E_{\mathrm{a}}}^{0}(Y_i) + \sum_{j}\Delta NNN_{E_{\mathrm{a}}j}^{0} \quad (5)$$

$$\mathrm{Log}\left(\tilde{A}\right) = \mathrm{Log}^{\mathrm{Ref}}\left(\tilde{A}\right) + \sum_{i=1}^{2}\Delta\mathrm{GAV}_{\mathrm{Log}\left(\tilde{A}\right)}^{0}(\mathrm{Si}_i) + \Delta\mathrm{GAV}_{\mathrm{Log}\left(\tilde{A}\right)}^{0}(X_1) + \sum_{i=1}^{2}\Delta\mathrm{GAV}_{\mathrm{Log}\left(\tilde{A}\right)}^{0}(Y_i) + \sum_{j}\Delta NNN_{\mathrm{Log}\left(\tilde{A}\right)j}^{0}, \quad (6)$$

where $\Delta\mathrm{GAV}^{0}$ is defined in Eq. 7:

$$\Delta\mathrm{GAV}^{0} = \mathrm{GAV}(\mathrm{TS}) - \mathrm{GAV}(\mathrm{reactants}) - \mathrm{GAV}(\mathrm{reference}). \quad (7)$$

The use of a reference reaction allows E_{a} and $\tilde{A}$ to be captured as structural deviations. Moreover, TSGA prediction accuracy can be improved easily in the future by recalculating E_{a} and $\tilde{A}$ for only the reference reaction, and most of the temperature dependence of the Arrhenius parameters is confined to the reference reaction, while the

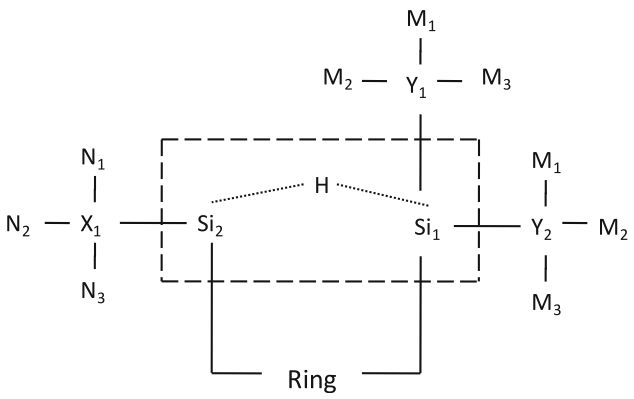

Fig. 4 Representative transition state of a cyclization/ring opening reaction where the dashed box is the reactive center. X and Y are primary contributions. N and M are secondary interactions

group additivity values are largely temperature independent. This approach also reduces the combinatorial explosion that plagues previous approaches using supergroups when more structurally diverse reactants are included. Disilylsilylene isomerization to cyclotrisilane was chosen as the reference reaction (Fig. 1) because it is the simplest reaction in the class and the structure of the reactive center does not deviate considerably from the other reactions in the training set.

A more simplified formulation of TSGA was also explored. As shown in Eqs, 8 and 9, it was possible to include only primary contributions to predict Arrhenius parameters. This approximation was used successfully in hydrocarbon chemistry [71–73] and in our work in which substituted silylene–silene isomerization and silylene addition and elimination were examined [89, 98].

$$E_a = E_a^{Ref} + \sum_{i=1}^{2} \Delta GAV^0_{E_a}(Si_i) \tag{8}$$

$$Log(\tilde{A}) = Log^{Ref}(\tilde{A}) + \sum_{i=1}^{2} \Delta GAV^0_{Log(\tilde{A})}(Si_i). \tag{9}$$

The primary silicon atoms were differentiated according to the number of Si and H atoms to which they were attached. The five primary contributions to the reactive center used in TSGA were: (1) Si_1–$(H)_3$, (2) Si_1–$(Si)(H)_2$, (3) Si_1–$(Si)_2(H)$, (4) Si_2–(H) and (5) Si_2–(Si). A ring correction was included and dependent on the size of the ring formed or dissociated. When a molecule contained a single ring, inclusion of ring corrections was straightforward. However, when multiple rings were present for a given silicon hydride, only the ring correction associated with the ring size formed or dissociated was used because the effect on the reactive center dominates the structural changes of the silicon hydride. For example in Fig. 3, bicyclo[3.1.0]hexasilane formed in reaction 25 was assigned only one three-membered ring correction. This strategy reduces the number of parameters needed for the estimation of E_a and $\tilde{A}$ while still capturing the data accurately.

To develop the TSGA parameters, the training set shown in Fig. 2 was used. The reactions are shown using notation typically used for hydrocarbons, but each multivalent atom depicted is a silicon atom, which contains the identical number of valence electrons as carbon. The silicon hydrides in the training set had a maximum of eight silicon atoms. In Fig. 2, reactions 1 through 4 explore the formation of rings with only hydrogen substituents on the reactive center. Reactions 5 through 8 explore the formation of rings from a secondary substituted silylene. Reactions 9 through 12 explore the formation of rings when the donating silicon atom is secondary. Reactions 13 through 16 explore the formation of rings when the donating silicon atom is tertiary. Rings larger than six silicon atoms were not examined because (1) larger systems are computationally more intensive for quantum chemical calculations and (2) crystalline silicon without defects will assume a diamond cubic structure where six-membered rings form a series of hexagonal channels, and larger ring sizes are thermodynamically unfavored [99, 100]. Moreover, this study has predicted a net formation of three-, four- and five-membered rings in hydrogenated amorphous silicon nanostructures (see "Results and discussion").

The TSGA parameters were obtained using multiple linear regression with the least squares method for all training set reactions. The overall model was deemed significant if the F test satisfied the 90% confidence level (i.e., the P value was below $\alpha = 0.10$). The significance of each TSGA parameter of the model was then determined with a t test at the 90 and 95% confidence levels. All insignificant parameters were removed from the model. Four six-parameter databases were obtained from 16 training set reactions: one each for E_a and log $\tilde{A}$ of the cyclization and ring opening reactions. The TSGA parameter databases were then validated against nine reactions that were not included in the training set. These validation set reactions are displayed in Fig. 3. The molecules comprising the validation set reactions are either polycyclic or explore steric hindrances across the reactive center.

Finally, the results from the TSGA method were compared with the prediction of $\tilde{A}$ and E_a from the kinetic correlations in the literature generalized from silylene addition and elimination reactions, which are based on a representative value for the pre-exponential factor ($\tilde{A}_{\text{ring opening}} = 2 \times 10^{15}\ s^{-1}$) [1, 66] and the Evans–Polanyi correlation ($E_a = E_o + \gamma\,\Delta H_{Rxn}$; $E_o = 0$ kcal mol^{-1}; $\gamma = 0$ for cyclization; $\gamma = 1$ for ring opening) [2, 65], respectively.

3 Results and discussion

3.1 The presence of a cyclic intermediate

A total of 25 cyclization/ring opening reactions were mapped using G3//B3LYP. Mapping of the cyclization/ring opening potential energy surface for all the reactions showed two distinct barriers linked by a common cyclic intermediate, which is a stable 1,3-, 1,4-, 1,5- or 1,6-hydrogen-bridged species for three-, four-, five- and six-membered ring formation reactions, respectively, as depicted in Fig. 1 for disilylsilylene isomerization to cyclotrisilane. There is no experimental evidence for the intramolecular formation of a hydrogen-bridged intermediate for ring formation reactions; however, there is experimental evidence for the

intermolecular formation of a hydrogen-bridged intermediate for the reaction of silylene and monosilane to form disilane by Becerra et al. [101] and the intramolecular formation of a hydrogen-bridged intermediate for the isomerization of silylsilylene to disilene by McCarthy et al. [102]. A summary of the standard enthalpies of reaction for the conversion of the substituted silylene to a cyclic intermediate and the conversion of the cyclic intermediate to a cyclic silane is given in Table 2.

The formation of the stable intermediate from the substituted silylene is always exothermic. The intermediate formation is associated with the torsional and scissoring normal vibrational modes along the backbone of Si–Si σ bonds of the substituted silylene. The average standard enthalpy of reaction for the first step for all the reactions of Figs. 2 and 3 was -10 kcal mol^{-1}, where the most exothermic cyclic intermediate formation was -14 kcal mol^{-1} for reaction 16. The formation of a cyclic intermediate from a substituted silylene was more exothermic for the formation of larger rings as the heats of reactions ranged from -6 to -10 kcal mol^{-1} for three- and four-membered ring formation reactions and -11 to -14 kcal mol^{-1} for five- and six-membered ring formation reactions. A plot of the temperature dependence of ΔG_{Rxn} values for the conversion of the substituted silylene to the cyclic intermediate for several key reactions is provided in Fig. 5b. ΔG_{Rxn} values for the conversion of the substituted silylene to the cyclic intermediate increase with increasing temperature, or the equilibrium shifts to favor substituted silylenes for all ring sizes; moreover, the least steep shift is for smaller rings. At 298 K, ΔG_{Rxn} values for the conversion of the substituted silylene to the cyclic intermediate for all ring sizes are similar.

Table 2 Enthalpy of reaction at 298 K and 1 atm for formation of the cyclic intermediate from a substituted silylene reactant (step 1) and conversion of the cyclic intermediate to form the cyclic silicon hydride product (step 2)

Reaction	$\Delta H^{298}_{\mathrm{Rxn}}$ (kcal mol^{-1})	
	Step 1	Step 2
1	−6.3	−11.9
2	−7.3	−32.9
3	−11.5	−39.6
4	−11.7	−44.1
5	−8.3	−11.8
6	−7.3	−33.5
7	−12.2	−39.7
8	−10.9	−45.7
9	−7.9	−13.5
10	−8.0	−34.1
11	−12.0	−41.2
12	−12.7	−45.3
13	−9.6	−14.7
14	−8.8	−35.3
15	−13.1	−42.8
16	−14.0	−46.5
17	−9.2	−15.6
18	−11.2	−44.5
19	−8.2	−34.1
20	−6.9	−34.1
21	−12.1	−41.2
22	−10.9	−39.1
23	−11.9	−44.2
24	−9.5	−14.4
25	−10.3	−12.7

The conversion of the cyclic intermediate to a saturated cyclic silicon hydride is also very exothermic, revealing that the intermediate is enthalpically uphill from the cyclic silicon hydride product. The standard enthalpy of reaction ranged from -12 to -47 kcal mol^{-1} for all of the reactions. The most exothermic conversion of the cyclic intermediate to a saturated cyclic silicon hydride was for reaction 16. A plot of the temperature dependence of ΔG_{Rxn} values for the conversion of the cyclic intermediate to the saturated cyclic silicon hydride product for several key reactions is provided in Fig. 5c. The ring size formed from the cyclic intermediate has a pronounced effect on ΔG_{Rxn} values. ΔG_{Rxn} values for the conversion of the 1,3-hydrogen-bridged cyclic intermediate to a three-membered ring decrease with increasing temperature. ΔG_{Rxn} values for the conversion of cyclic intermediates to four-, five-, and six-membered rings increase with increasing temperature; however, ΔG_{Rxn} values for the conversion of the 1,5-hydrogen-bridged cyclic intermediate to a five-membered ring change the least over the temperature range of 298–1,500 K. Interestingly, the equilibrium concentration distribution only shifts to favor three-membered ring formation reactions from the cyclic intermediate with increasing temperature.

A plot of the temperature dependence of the standard Gibbs free energy of the reaction for the overall conversion of the substituted silylene to a cyclic silicon hydride product for several key reactions is provided in Fig. 5a. As temperature is increased, ΔG_{Rxn} values for the overall conversion of the substituted silylene to the cyclic silicon hydride product increase. The overall conversion of substituted silylenes to form six-membered rings has the steepest change in ΔG_{Rxn} values as temperature is increased. The shift in equilibrium concentration distribution with an increase in temperature will cause the acyclic substituted silylene to become more favorable in each case; however, the distribution of three-membered ring and disilylsilylene concentrations will show very little shift over the temperature range of 298–1,500 K.

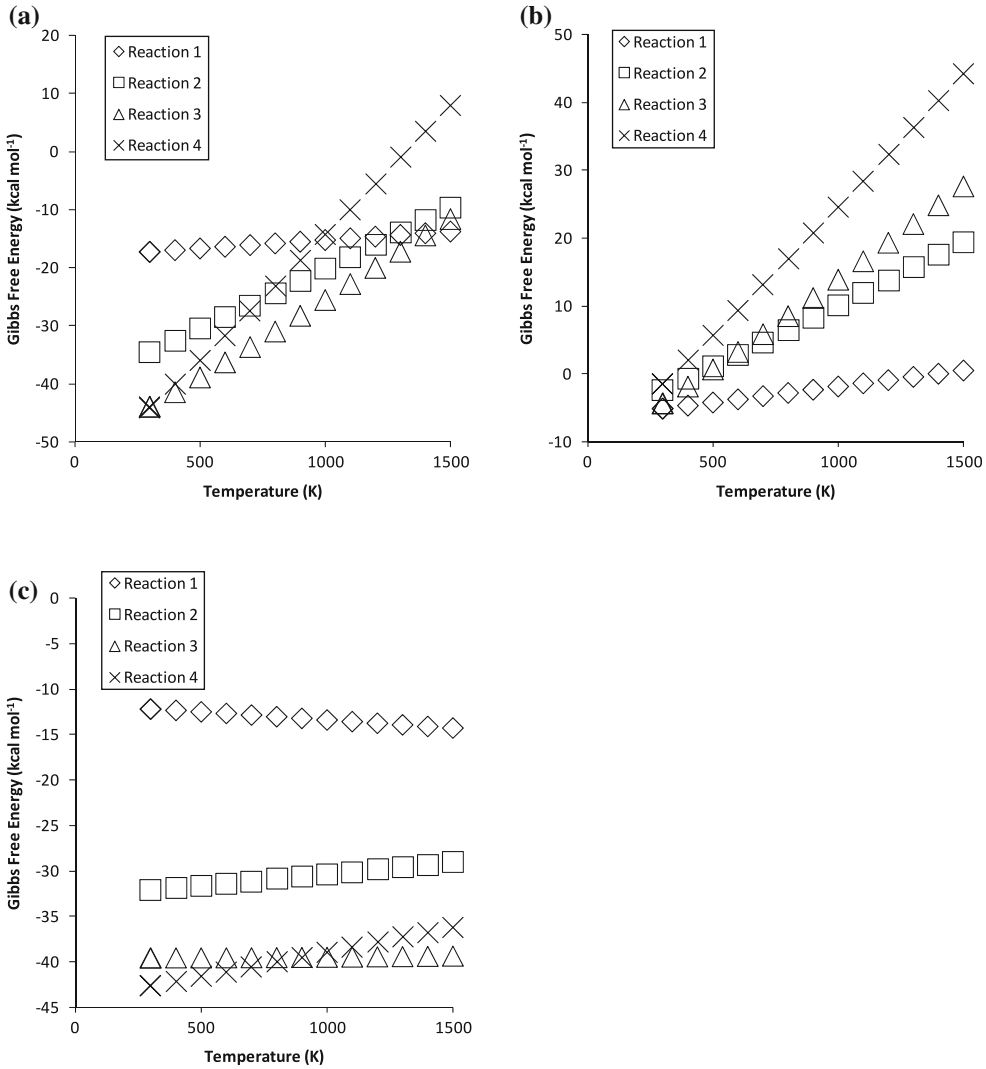

Fig. 5 Ring size effects on the standard Gibbs free energy of reaction for several key cyclization reactions: **a** substituted silylene to cyclic silicon hydride, **b** substituted silylene to cyclic intermediate and **c** cyclic intermediate to cyclic silicon hydride

3.2 Internal rotation corrections

Normal vibrational modes that were more appropriately treated as free rotations that do not cancel out between the reactant and the transition state were treated using a one-dimensional internal rotation model. For example, the cyclization reactions involving three- to six-membered rings have between two and five potential internal rotations, respectively, between the donor silicon atom and the divalent center along the backbone Si–Si σ bonds in the substituted silylene that are not present in the cyclic silicon hydride product. The non-canceling internal rotations are only present in the substituted silylene. Using Fig. 6a as an illustrative model, the two non-canceling internal rotations in the substituted silylene for the three-membered ring cyclization reaction are about the bonds formed by atoms 1–2 and 2–3.

Treating internal rotations as free rotations is a valid approximation for pyrolytic conditions as the barriers to rotation for Si–Si σ bonds in silicon hydrides are on average under 1 kcal mol^{-1}. The transition from a hindered to a free rotor, where k_BT equals the maximum barrier height to internal rotation, on average occurs at temperatures well below pyrolytic conditions so the free rotor approximation is valid. To confirm this hypothesis, potential energy surface scans using B3LYP/6-31G(d) were performed on the internal rotations for several silicon hydrides. The barriers to rotation along the backbone of Si–Si σ bonds for disilane and trisilane are 0.91 and 0.77 kcal mol^{-1}, respectively. Substituted silylenes such as H_3Si–Si:H and H_3Si–$(SiH_2)_3$–Si:H had small barrier heights to rotation for the Si–Si bond adjacent to the divalent center as well, with values of 0.25 and 1 kcal mol^{-1}, respectively. The remaining barrier heights to rotation in these two substituted silylenes are similar to those for saturated silicon hydrides. Moreover, a detailed treatment of anharmonic effects including anharmonic ring movements and internal rotations by Katzer et al. [42] for

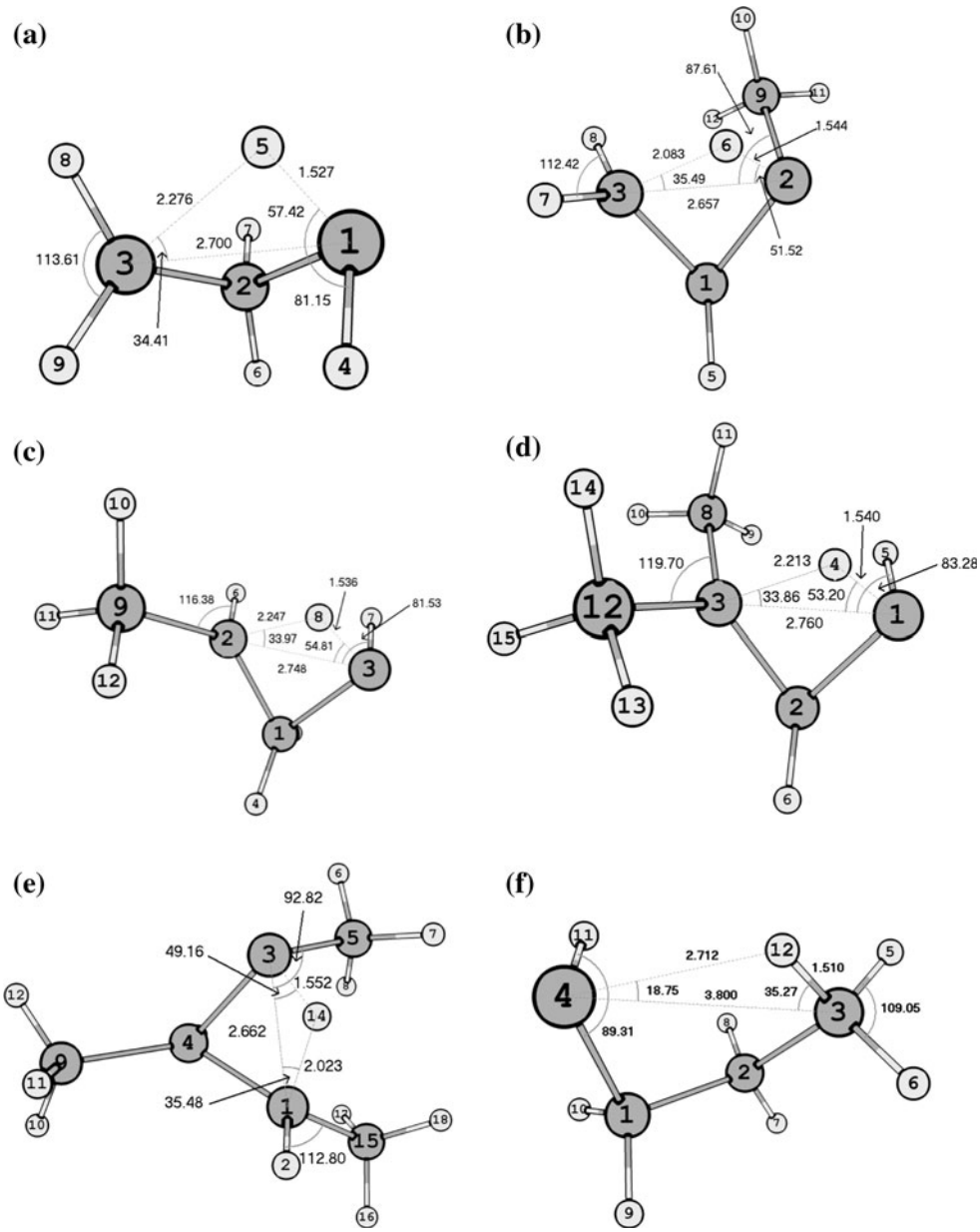

Fig. 6 B3LYP/6-31G(d) optimized geometries of the lowest energy conformer of the rate-determining transition state for several key reactions: **a** no silyl groups, **b** silyl group on Si_2, **c** one silyl group on Si_1, **d** two silyl groups on Si_1, and **e** steric interaction of silyl groups across the reactive center to form a three-membered ring, as well as **f** no silyl groups to form a four-membered ring. Si_1 and Si_2 notation correspond to that in Fig. 4. **a** The reference reaction. Distances are shown in Å

the ΔG_{Rxn} of the cyclization reaction to form cyclopentasilane was captured very well by our free rotor approximation alone. For example, our study and the work of Katzer et al. both predict the anharmonic correction to the ΔG_{Rxn} of the cyclization reaction to form cyclopentasilane to be approximately +12 kcal mol^{-1} at 1,000 K. This scheme to capture anharmonic effects was extended to all reactions in Figs. 2 and 3.

Table 3 summarizes the results of internal rotation corrections for the cyclization reaction. For the training set reactions of Fig. 2, the internal rotation correction lowers the rate coefficient for all four-, five-, and six-membered cyclization reactions by average factors of 5.2×10^{-2}, 1.3×10^{-3}, and 5.8×10^{-5}, respectively, at 1,000 K and 1 atm. For three-membered cyclization reactions at 1,000 K and 1 atm, primary divalent centers will have an internal rotation correction that increases the rate coefficient by an average factor of 7.1. Conversely, for a secondary divalent center, the rate coefficient is decreased by a factor of 0.11. The largest factors of change in the rate coefficient for the cyclization reactions due to internal rotation corrections were for six-membered ring formations; moreover, six-membered ring cyclization reactions from secondary divalent centers corrected for internal rotations had the highest deviations compared to the harmonic oscillator model (i.e., reaction 8). For both the

Table 3 Relative differences of Arrhenius parameters and rate coefficients at 1,000 K and 1 atm showing the effect of internal rotation corrections for cyclization reactions

Reaction	$\tilde{A}^{IR}/\tilde{A}^{HO}$	$E_a^{IR} - E_a^{HO}$ (kcal mol^{-1})	k^{IR}/k^{HO} (1,000 K)
1	7.2E+00	−0.1	7.54E+00
2	6.2E−02	−0.7	8.77E−02
3	1.2E−03	−1.3	2.29E−03
4	2.5E−05	−1.9	6.23E−05
5	1.1E−01	−0.1	1.13E−01
6	8.3E−04	−0.7	1.18E−03
7	1.5E−05	−1.3	2.95E−05
8	2.2E−07	−1.9	5.68E−07
9	7.9E+00	0.0	7.98E+00
10	4.3E−02	−0.6	5.83E−02
11	9.3E−04	−1.2	1.70E−03
12	6.2E−05	−1.7	1.48E−04
13	5.8E+00	0.0	5.81E+00
14	4.4E−02	−0.6	5.93E−02
15	5.8E−04	−1.2	1.05E−03
16	8.1E−06	−1.8	1.98E−05
17	2.4E+00	0.0	2.41E+00
18	1.3E−05	−1.8	3.31E−05
19	5.9E−02	−0.6	7.96E−02
20	4.9E−02	−0.6	6.66E−02
21	3.9E−06	−1.2	7.08E−06
22	1.1E−03	−1.3	2.08E−03
23	1.4E−05	−1.8	3.65E−05
24	3.2E−02	0.0	3.21E−02
25	1.4E+01	0.4	1.15E+01

training and test set, the cyclization reactions on average showed the log $\tilde{A}$ values and E_a to decrease 22% and 1 kcal mol^{-1}, respectively.

3.3 Rate-determining step

While our calculations reveal that the cyclic intermediate is clearly stable, it is unwieldy to have to track it explicitly in mechanistic models, as schemes for predicting the properties of these intermediates are not available. It is more convenient to consolidate the multiple step cyclization reaction and its reverse reaction into one overall transformation. The overall cyclization reactions are all exothermic; moreover, the exothermicity increases with an increase in the ring size formed. Prior to the consolidation of the two-step conversion, the rate-determining step was first validated by monitoring the reaction dynamics of reactions 1 through 4. Three microkinetic models for each reaction were created assuming: (1) a full model, (2) that the second step is rate-determining, and (3) that the first step is rate-determining. Model 1 explicitly includes the kinetic parameters for both elementary steps without assuming a rate-determining step. The rate coefficient to form the cyclic intermediate from the substituted silylene was calculated using one-dimensional variational TST [96, 97]. The overall rate coefficient for model 2 was calculated as $k = K_1 k_2$, where K_1 is the equilibrium coefficient for the first step, and k_2 is the rate coefficient for the second step. Model 3 calculates the overall rate coefficient as $k = k_1$, where k_1 is the rate coefficient for the first step. Over the temperature range of 750–1,200 K, model 2 is superior in predicting the reaction dynamics of the full model for reaction 1. When the temperature is below this range, model 3 outperforms model 2 for reaction 1, as the rate-determining step changes. Thus, three-membered ring formation and its reverse reaction were assumed to be controlled by the second step as the rate-determining step under pyrolysis conditions. For reactions involving three-membered ring formation in Figs. 2 and 3, the transition states were located using the QST3 potential energy surface interpolation method for the rate-determining step (i.e., the second barrier in the cyclization direction). Over the temperature range of 750–1,200 K, model 3 is superior in predicting the reaction dynamics of the full model for reactions 2–4. When the temperature is above this range, model 2 outperforms model 3 for reactions 2–4, as the rate-determining step changes. Thus, four-, five-, and six-membered ring formation and the reverse reactions were assumed to be controlled by the first step as the rate-determining step under pyrolysis conditions. For reactions involving four-, five- and six-membered ring formation in Figs. 2 and 3, the rate coefficients were calculated using one-dimensional variational TST for the rate-determining step (i.e., the first barrier in the cyclization direction).

Figure 6 shows the rate-determining transition state geometries for several key reactions. The structural changes upon addition of various substituents to either side of the reactive center can be seen by comparing these geometries. Similar to the singlet carbenes of hydrocarbon chemistry, the presence of an sp^2-hybridized divalent silicon center strains the angle made by the two central substituents. The unhindered acyclic substituents do not change the reactive center greatly (Fig. 6a–d); however, when there are silyl substituents on both sides of the reactive center, the steric hindrance of these groups plays a role in cyclization and ring opening reactions (Fig. 6e). The structure of the reactive center changes the most as the ring formed or dissociated becomes smaller, i.e., bond angles are closer to a tetrahedral geometry in the transition state for reactions involving the formation of larger rings. The cyclization reactions of ring sizes larger than three silicon atoms involve a looser transition state, as depicted in Fig. 6f for the formation of a four-membered ring.

This study concentrates on pyrolytic conditions and the impact of tunneling and above-the-barrier reflection is approximated by the Wigner tunneling correction. All of the reactions in Figs. 2 and 3 were treated using the same approach, and a summary of the zero point corrected energy barriers, the regressed E_a and $\tilde{A}$ values for the overall transformations, and the standard enthalpies of reaction for the formation of the cyclic silicon hydride product from a substituted silylene including internal rotation corrections is given in Table 4.

Over the temperature range of this study, the cyclization reactions have negative apparent activation energies. The most negative apparent activation energy of −7.14 kcal mol^{-1} is for reaction 25. Above the range of temperatures used in the linear regression for activation energies, the overall apparent activation energies for larger ring formation reactions become most negative, as the rate-determining step for the formation of four-, five- and six-membered rings in the cyclization direction becomes the second barrier. For ring opening reactions, classic Arrhenius behavior is observed. The Arrhenius temperature dependence of the rate coefficient for the ring opening reactions of cyclic silicon hydrides to form substituted silylenes is linear over all temperatures.

3.4 Ring statistics

Ring statistics quantify the medium-range order in amorphous materials by analyzing the atomic connectivity, and thus the concentration of different ring sizes in small nanostructures can be predicted [103]. Ring statistics for amorphous silicon are most commonly calculated from a radial distribution function generalized from X-ray or neutron scattering experiments [104] or computer simulations [36]. In our case, direct analysis of the prevalence of different molecular species was made to predict the internal connectivity of larger nanostructures. The formation of rings in polycyclic species was found to be largely dependent on the immediate ring size formed rather than the ring size present in the substituted silylene

Table 4 Arrhenius parameters, zero point energy corrected barriers and enthalpy of reaction at 298 K and 1 atm corrected for internal rotations

Reaction	Cyclization				Ring opening		
	E_o (kcal mol^{-1})	Log $\tilde{A}$	E_a (kcal mol^{-1})	ΔH^{298}_{Rxn} (kcal mol^{-1})	E_o (kcal mol^{-1})	Log $\tilde{A}$	E_a (kcal mol^{-1})
1	−0.8	12.45	−1.0	−18.1	16.8	13.08	17.2
2	−1.2	9.54	−2.1	−40.2	37.7	14.02	38.6
3	−0.4	8.38	−1.8	−51.1	48.9	14.14	50.1
4	0.0	6.18	−2.0	−55.8	53.6	15.51	55.1
5	−4.1	10.12	−4.5	−20.2	15.5	12.61	15.6
6	−1.9	8.03	−2.7	−40.8	37.7	13.83	38.5
7	−0.6	6.20	−2.0	−51.9	49.6	14.09	50.7
8	−0.4	4.22	−2.3	−56.7	54.2	15.22	55.4
9	−3.5	11.89	−3.7	−21.3	17.3	13.05	17.7
10	−1.0	10.00	−1.7	−42.1	40.0	14.15	40.9
11	−0.7	7.88	−1.9	−53.3	51.0	14.15	52.2
12	0.5	6.20	−1.4	−58.1	56.5	15.53	57.8
13	−6.8	12.11	−7.0	−24.3	17.1	13.01	17.4
14	−0.9	9.98	−1.6	−44.2	42.2	14.06	43.1
15	−1.3	7.40	−2.6	−55.8	53.1	14.18	54.1
16	−0.5	4.73	−2.4	−60.5	58.0	15.12	59.2
17	−6.9	12.02	−7.0	−24.8	17.4	13.05	17.9
18	1.0	5.98	−0.8	−55.7	54.5	15.26	56.1
19	−0.7	9.81	−1.4	−42.3	40.5	14.20	41.5
20	0.2	9.44	−0.6	−41.0	40.0	14.11	40.9
21	−0.7	5.52	−2.0	−53.3	51.2	14.00	52.0
22	−0.8	7.82	−2.2	−50.0	47.5	13.98	48.6
23	0.4	6.22	−1.5	−56.2	54.3	15.44	55.8
24	−6.9	9.64	−7.1	−23.9	16.6	12.82	16.9
25	−7.1	11.46	−7.1	−23.0	15.3	13.07	15.6

The kinetic parameters were calculated assuming that the first step in the cyclization direction is equilibrated for three-membered ring formation, and the second step in the cyclization direction is equilibrated for four-, five- and six-membered ring formations. $\tilde{A}$ has units of s^{-1}

(e.g., reaction 25). Therefore, ring formation reactions in polycyclic species are generalized from monocyclic ring formation reaction kinetics. The need for internal rotation corrections will be lessened as the ratio of silicon-to-hydrogen atoms becomes greater in a larger nanostructure. Due to restricted atomic movements, the divalent centers in the core of the nanostructure are well described by the harmonic oscillator model for normal vibrational modes.

Figure 7 shows interesting trends depending on ring size by way of Arrhenius plots for the cyclization and ring opening pathways of reactions 1 through 4. The rate coefficients of the cyclization reactions of three-, four-, five- and six-membered rings all decrease with increased temperature. As the ring size formed is increased, the Arrhenius plots for cyclization over the temperature range of this study become more convex. Smaller ring formation reactions are faster than larger ring formation reactions. For the reverse reaction, smaller ring opening reactions are faster than larger ring opening reactions. Because larger rings approach tetrahedral bond angles for the silicon atoms confined to the ring, the ring opening rate coefficients of five- and six-membered rings are nearly identical over the temperature range of this study. Figures 8 and 9 show the correlations between ln k, log $\tilde{A}$ and E_a and ring size for all of the training set reactions (Fig. 2) for cyclization and ring opening, respectively. With an increase in the ring size formed, ln k decreases linearly, E_a reaches an asymptotic value, and log $\tilde{A}$ decreases for the cyclization of all training set reactions. Similarly, for the reverse reaction, ln k decreases exponentially and E_a increases asymptotically, while log $\tilde{A}$ increases on average with an increase in the ring size formed.

Figure 10 presents ring size effects on the equilibrium concentration distributions of cyclic silicon hydrides and acyclic substituted silylenes for several key reactions at various temperatures. Internal rotation corrections have a large impact on equilibrium concentration distributions for hydrogenated amorphous silicon nanostructures with high hydrogen to silicon atom ratios. Figure 10a clearly provides the first quantum chemical calculations that offer evidence for the preferred formation of cyclopentasilane instead of larger ring sizes at low temperatures [7–9]. At 750 K, four- and five-membered rings will have the highest equilibrium concentrations in silicon hydrides. At higher temperatures (750–1,200 K), three-membered rings will also be present to a greater degree in silicon hydride nanostructures. This increase in the equilibrium concentration of smaller rings will decrease the average internal Si–Si–Si bond angle of hydrogenated silicon nanostructures significantly. Higher temperatures will also decrease the equilibrium concentration ratio of cyclic silicon hydrides to acyclic substituted silylenes.

These quantum chemical data also suggest average internal Si–Si–Si bond angles to be less than 90° for highly compressed nanostructures containing high hydrogen content. Assuming nearly equal concentrations of three-, four- and five-membered rings in hydrogenated silicon nanostructures at temperatures between 1,000 and 1,200 K (containing Si–Si–Si bond angles of approximately 60°, 88° and 105°, respectively), the average internal Si–Si–Si bond angle is predicted to be approximately 84°. This prediction is supported by the computational studies of Galashev et al. [36] where molecular dynamics calculations on larger silicon structures (i.e., $Si_{73}H_{60}$) exhibit internal silicon atom bond angles averaging 90° compared to bulk amorphous silicon where internal silicon atom bond angles are on average 109° ± 10° generalized from X-ray scattering experiments [104]. Hydrogen content of silicon

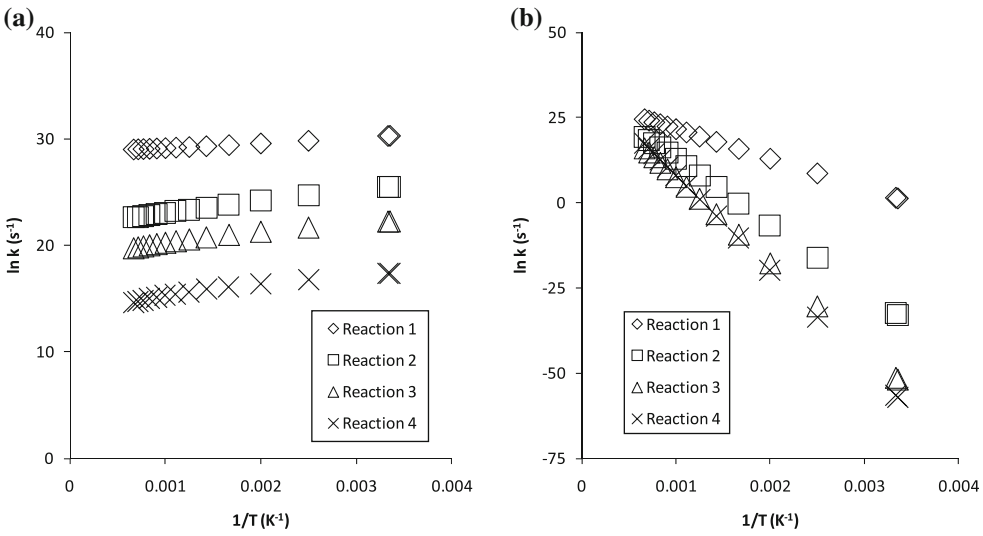

Fig. 7 Arrhenius plots comparing rate coefficients as a function of ring size for: **a** cyclization and **b** ring opening

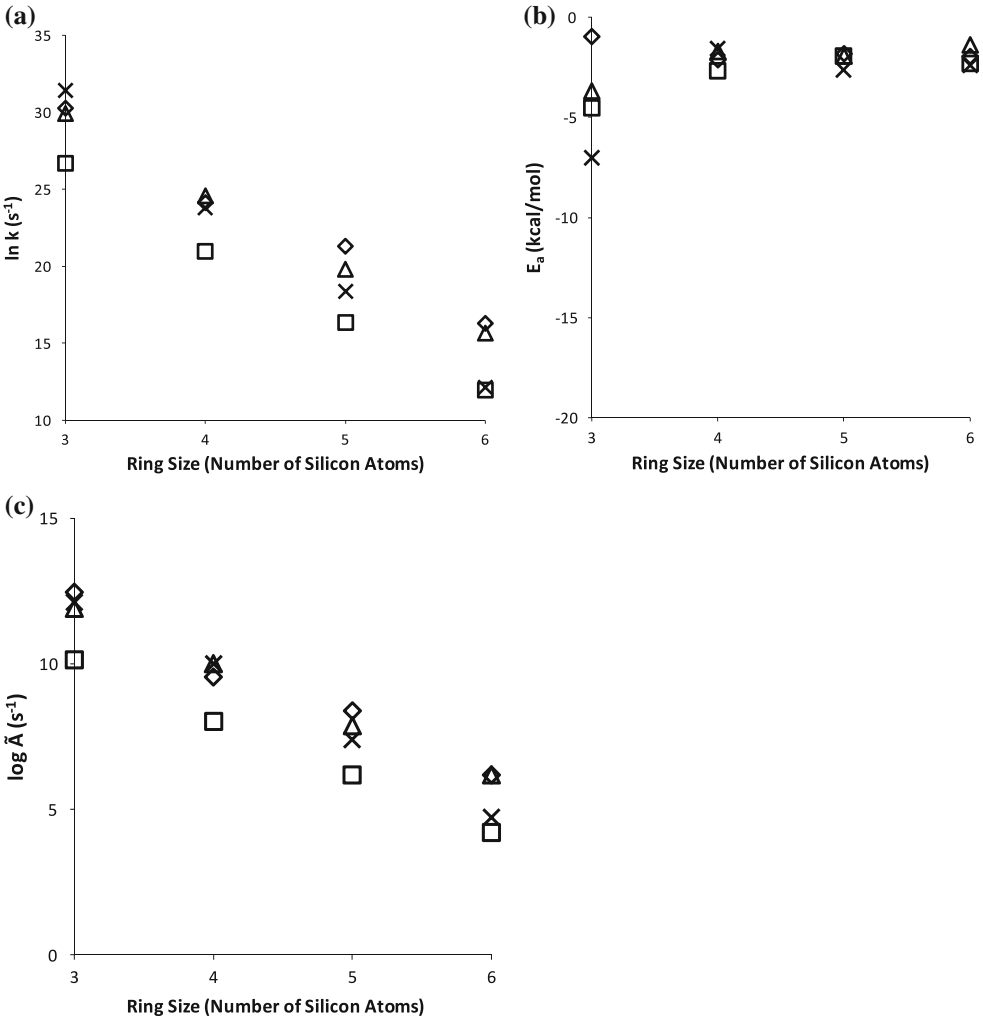

Fig. 8 Ring size effects on kinetic parameters for several key cyclization reactions: **a** rate coefficient at 1,000 K and 1 atm, **b** E_a, and **c** log $\tilde{A}$. The *diamonds* correspond to reactions 1–4. The *squares* correspond to reactions 5–8. The *triangles* correspond to reactions 9–12. The Xs correspond to reactions 13–16

hydrides has a clearly compressive effect on cyclic structure and smaller Si–Si–Si bond angles internally will be favored.

3.5 TSGA parameters

TSGA parameters were regressed from the training set reactions of Fig. 2. The matrices used to derive the TSGA parameters were constructed using a sum of the primary contributions to the reactive center and one ring correction for each reaction. Table 5 summarizes the results of various least squares regressions for E_a, and Table 6 summarizes the same information for log $\tilde{A}$. The full parameter model contains six parameters. The TSGA group values for the full model are summarized in Tables 5a and 6a for E_a and log $\tilde{A}$, respectively. Parity plots depicting how well the full model captures the training set values of the rate coefficients at 1,000 K and 1 atm, E_a, and log $\tilde{A}$ for cyclization and ring opening reactions are shown in Figs. 11a–c and 12a–c, respectively. The values predicted by the kinetic correlations in the literature are also provided for comparison. Standard enthalpies and Gibbs free energies of reaction corrected for internal rotations were used for the Evans–Polanyi correlation (Figs. 12b, 14b) and the subsequent calculation of the reverse rate coefficients for cyclization (Figs. 11a, 13a), respectively. The log $\tilde{A}$ values presented in Figs. 11c and 13c were back calculated from the reverse rate coefficients for cyclization based on the principle of thermodynamic reversibility. The internal rotations were included in our comparison to focus upon the predictive capacity of the kinetic correlations and the representative log $\tilde{A}$ value and not the impact of internal rotation corrections. It is clear from these plots that the ability of TSGA to capture the k values at 1,000 K is only slightly superior to that of the literature correlations. This result is due to the incorporation of internal rotation corrections for the thermodynamic properties used in the kinetic correlations from literature. The use of thermodynamic properties not corrected for internal rotations will significantly decrease the predictive accuracy of the kinetic correlations from literature. However, the ability of TSGA to capture E_a and log $\tilde{A}$ is clearly superior. For the training

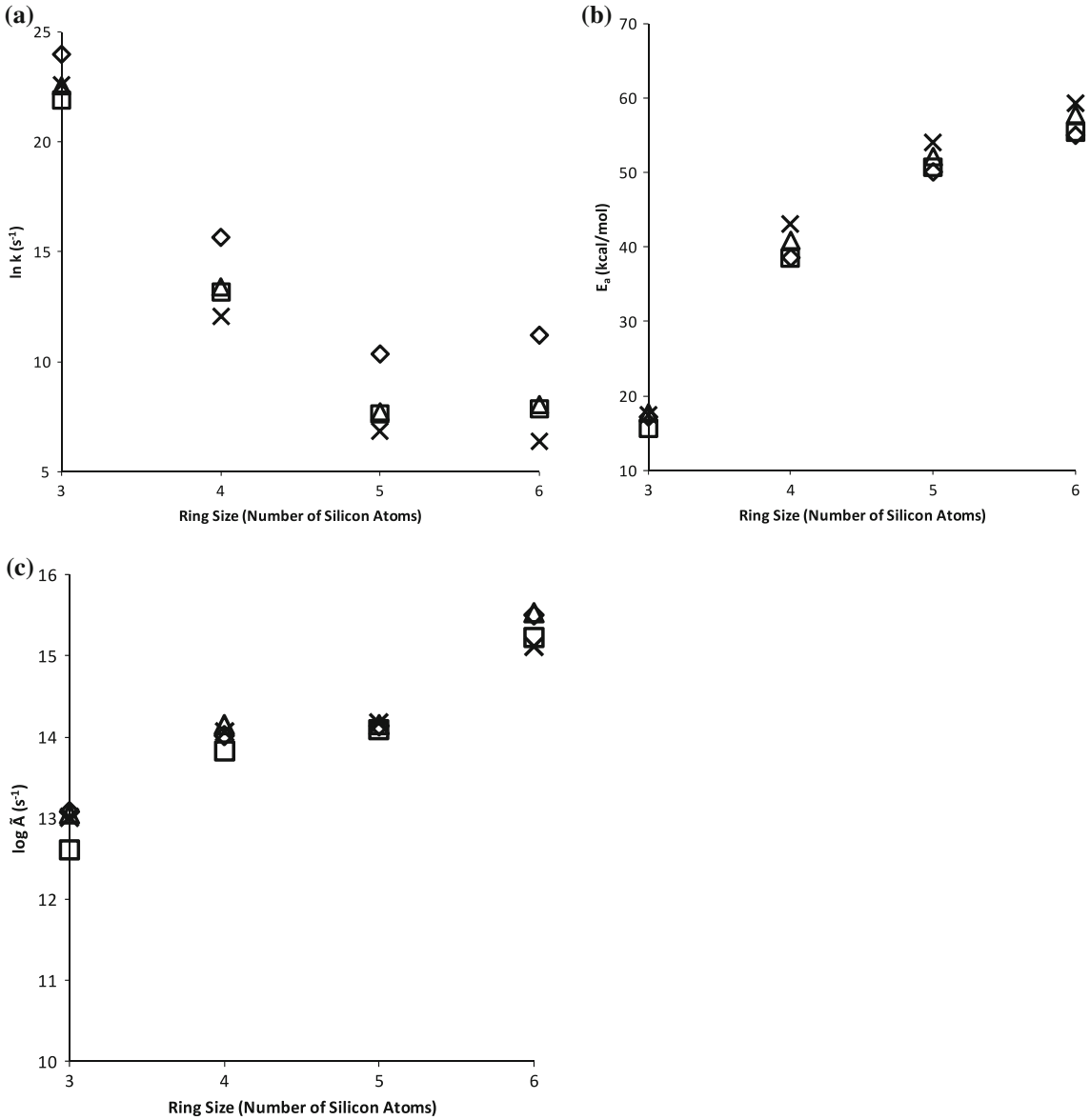

Fig. 9 Ring size effects on kinetic parameters for several key ring opening reactions: **a** rate coefficient at 1,000 K and 1 atm, **b** E_a, and **c** log $\tilde{A}$. The *diamonds* correspond to reactions 1–4. The *squares* correspond to reactions 5–8. The *triangles* correspond to reactions 9–12. The Xs correspond to reactions 13–16

set reactions, the mean absolute deviation values for the prediction of G3//B3LYP values with the TSGA method for E_a and log $\tilde{A}$ are 0.64 and 0.97 kcal mol^{-1} and 0.08 and 0.25 for the ring opening and cyclization reactions, respectively. A performance summary for the cyclization and ring opening reactions is provided in Tables 7 and 8, respectively. The G3//B3LYP and TSGA rate coefficients for all training set reactions can be found in Supporting Information.

Two additional models were explored based on eliminating parameters from the full model that did not meet the *t* test statistic at the (1) 95% and (2) 90% confidence levels for log $\tilde{A}$ and E_a separately. According to the *F* test, all of the regressed models were statistically significant at the 90% confidence level. The statistics for these two models are summarized in Tables 5 and 6 for E_a and log $\tilde{A}$, respectively. The TSGA parameters for E_a are summarized in Table 5a and log $\tilde{A}$ values are summarized in Table 6a. For the prediction of E_a and log $\tilde{A}$ values using TSGA, the same parameters are statistically significant at the 90 and 95% confidence levels. For the prediction of E_a and log $\tilde{A}$ using TSGA, all parameters excluding primary contributions pertaining to a donating primary silicon center are necessary for a statistically significant model at the 95%

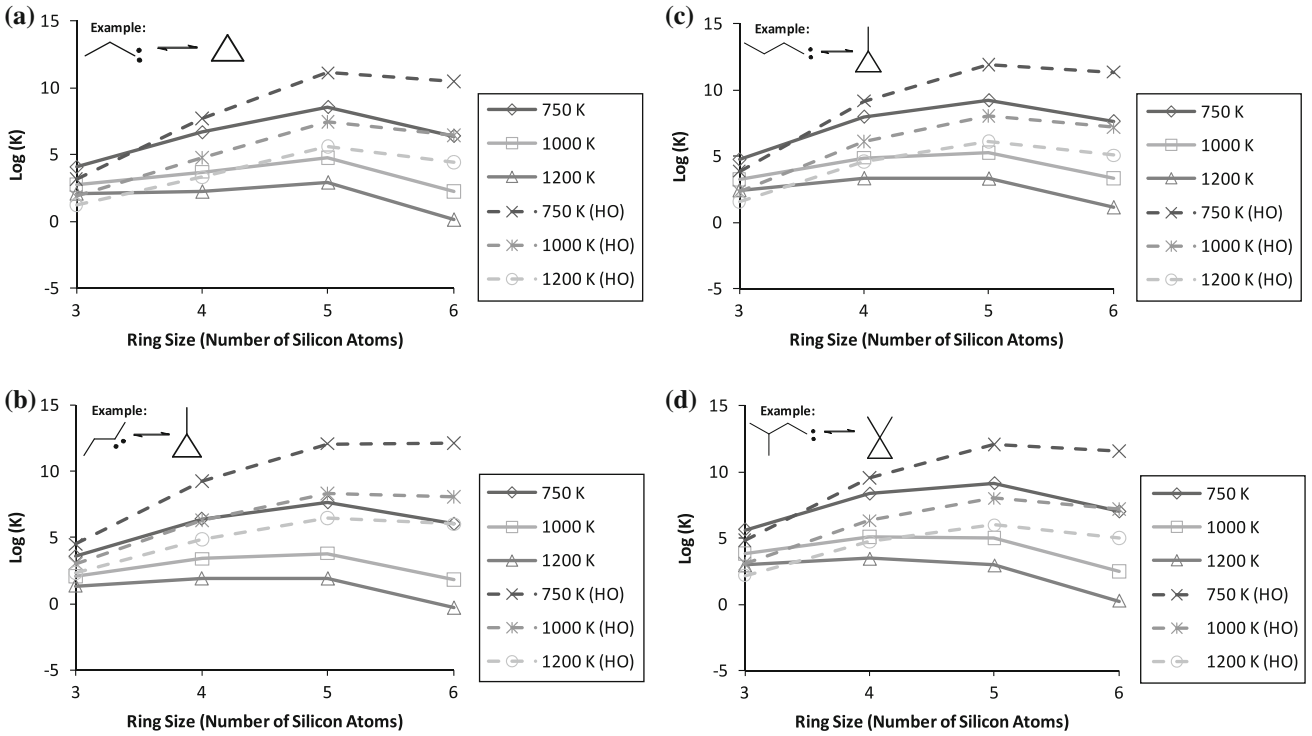

Fig. 10 Ring size effects on the equilibrium concentration distribution of cyclic silicon hydrides and acyclic substituted silylenes for several key cyclization reactions at 750, 1,000 and 1,200 K and 1 atm: **a** 1 through 4, **b** 5 through 8, **c** 9 through 12 and **d** 13 through 16. The *solid lines* represent equilibrium coefficients, K, corrected for internal rotations, and the *dashed lines* represent equilibrium coefficients calculated assuming the harmonic oscillator approximation with vibrational frequencies corrected by linear scaling factors. The equilibrium coefficient is unitless

confidence level. However, as summarized in Tables 5b and 6b, the goodness of fit is decreased in the case of cyclization compared to the full parameter model.

These more simplified models reveal that the reference reaction does not capture the single-event pre-exponential factor, $\tilde{A}$, for the cyclization and ring opening reactions well and pinpoint the more significant structural factors affecting the log $\tilde{A}$ value. TSGA parameters pertaining to the primary contributions to the reactive center (or addition of one silicon atom adjacent to the divalent center and two silicon atoms adjacent to the donor silicon atom) and ring corrections are statistically significant at the 95% confidence level. When transforming a substituted silylene to a cyclic silicon hydride species, addition of silicon atoms to the donor silicon atom or to the attacking silicon atom, as well as increasing the ring size formed, always decrease log $\tilde{A}$ values. In the reverse direction, the ring corrections and one primary contribution pertaining to the addition of a silicon atom to the attacking divalent center are statistically significant at the 95% confidence level; moreover, the addition of multiple silicon atoms to the donating silicon atom or one silicon atom adjacent to the divalent center decreases log $\tilde{A}$ values while increasing the ring size formed increases log $\tilde{A}$ values.

These analyses also reveal that the E_a values for substituted silylenes undergoing the cyclization reaction are not captured very well by the reference reaction alone. TSGA parameters pertaining to the primary contributions to the reactive center (or addition of one silicon atom adjacent to the divalent center and two silicon atoms adjacent to the donor silicon atom) are statistically significant at the 95% confidence level. When transforming a substituted silylene to a cyclic silicon hydride species, addition of silicon atoms to the donor silicon atom or the attacking silicon atom always decreases E_a, but increasing the size of the ring formed increases E_a. In the reverse direction, the ring corrections and one primary contribution pertaining to the addition of two silicon atoms to the donor silicon atom are statistically significant at the 95% confidence level; moreover, the addition of silicon atoms to the donating silicon atom or increasing the ring size formed increases E_a while addition of a silicon atom adjacent to the divalent center decreases E_a.

3.6 Validation of TSGA parameters

The TSGA parameters were then tested by comparing the predictions from the TSGA method against G3//B3LYP values for the validation reactions in Fig. 3. A

Table 5 (a) TSGA parameters for prediction of E_a at different levels of statistical significance, (b) statistical analysis for least squares regression of E_a TSGA parameters

(a) Reaction	Parameter (t test)	E_a (kcal mol^{-1})					
		Primary contributions			Ring correction		
	α-Level	Si_1-(Si)(H)$_2$	Si_1-(Si)$_2$(H)	Si_2-(Si)	Ring size		
					4	5	6
Cyclization	Full	−1.8	−3.0	−2.4	0.7	0.7	0.7
	$\alpha = 0.1$	*X*	−2.5	−1.9	*X*	*X*	*X*
	$\alpha = 0.05$	*X*	−2.5	−1.9	*X*	*X*	*X*
Ring opening	Full	1.1	2.4	−1.0	22.5	34.0	39.1
	$\alpha = 0.1$	*X*	2.4	*X*	22.5	34.0	39.1
	$\alpha = 0.05$	*X*	2.4	*X*	22.5	34.0	39.1

(b) Reaction	Parameter (t test)	E_a		
	α-Level	R^2 value	Regression F test	
			F value	P value
Cyclization	Full	0.653	3	0.079
	$\alpha = 0.1$	0.534	7	0.007
	$\alpha = 0.05$	0.534	7	0.007
Ring opening	Full	0.999	1771	<0.001
	$\alpha = 0.1$	0.998	1,803	<0.001
	$\alpha = 0.05$	0.998	1,803	<0.001

Table 6 (a) TSGA parameters for prediction of Log $\tilde{A}$ at different levels of statistical significance ($\tilde{A}$ has units of s^{-1}), (b) statistical analysis for least squares regression of Log $\tilde{A}$ TSGA parameters

(a) Reaction	Parameter (t test)	Log $\tilde{A}$					
		Primary contributions			Ring correction		
	α-Level	Si_1-(Si)(H)$_2$	Si_1-(Si)$_2$(H)	Si_2-(Si)	Ring size		
					4	5	6
Cyclization	Full	−0.2	−0.7	−2.1	−2.3	−4.3	−6.4
	$\alpha = 0.1$	*X*	−0.6	−2.0	−2.4	−4.3	−6.5
	$\alpha = 0.05$	*X*	−0.6	−2.0	−2.4	−4.3	−6.5
Ring opening	Full	0.0	−0.1	−0.3	1.0	1.2	2.4
	$\alpha = 0.1$	*X*	*X*	−0.3	1.0	1.1	2.3
	$\alpha = 0.05$	*X*	*X*	−0.3	1.0	1.1	2.3

(b) Reaction	Parameter (t test)	Log $\tilde{A}$		
	α-Level	R^2 value	Regression F test	
			F value	P value
Cyclization	Full	0.995	327	<0.001
	$\alpha = 0.1$	0.995	403	<0.001
	$\alpha = 0.05$	0.995	403	<0.001
Ring opening	Full	0.995	290	<0.001
	$\alpha = 0.1$	0.993	393	<0.001
	$\alpha = 0.05$	0.993	393	<0.001

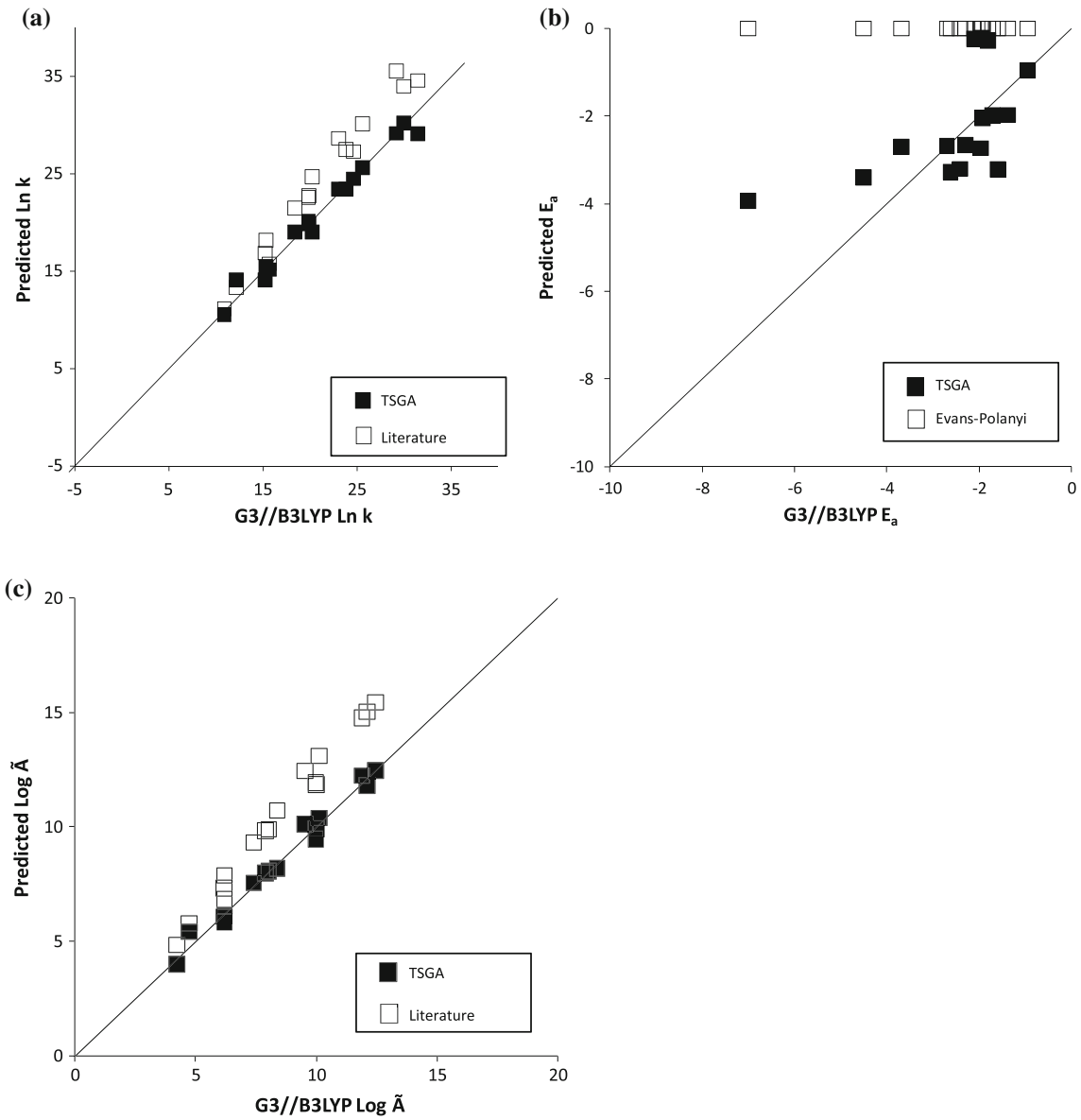

Fig. 11 Parity plots of cyclization for training reactions: **a** ln k at 1,000 K and 1 atm (units for k are s^{-1}), **b** E_a (units for E_a are kcal mol^{-1}), **c** log $\tilde{A}$ (units for $\tilde{A}$ are s^{-1})

performance summary for the cyclization and ring opening reactions is provided in Tables 9 and 10, respectively. The G3//B3LYP and TSGA rate coefficients for all validation set reactions can be found in Supporting Information. For 78% of the validation reactions in the temperature range of 750–1,200 K, the TSGA and G3//B3LYP rate coefficients were within an average factor of two for cyclization. For 89% of the validation reactions in the temperature range of 750–1,200 K, the TSGA and G3//B3LYP rate coefficients were within an average factor of two for ring opening. Reactions 17 and 21 deviated most significantly in the cyclization direction by factors of 0.13 and 8.8, respectively, at 1,000 K. In the ring opening direction, reaction 25 deviated the most by a factor of 0.10 at 1,000 K.

It is interesting to examine how well the cyclization and ring opening reactions for a polycyclic species are predicted by TSGA. A reaction involving a polycyclic species composed of smaller rings (e.g., reaction 25) is predicted reasonably well. For reaction 25, TSGA underpredicts the rate coefficient by a factor of 0.43 for cyclization and 0.10 for ring opening at 1,000 K.

The reactions involving the formation of a highly substituted smaller ring (e.g., reactions 17 and 20) with multiple tertiary silicon atoms in the ring formed are predicted well; TSGA only underpredicts and overpredicts the

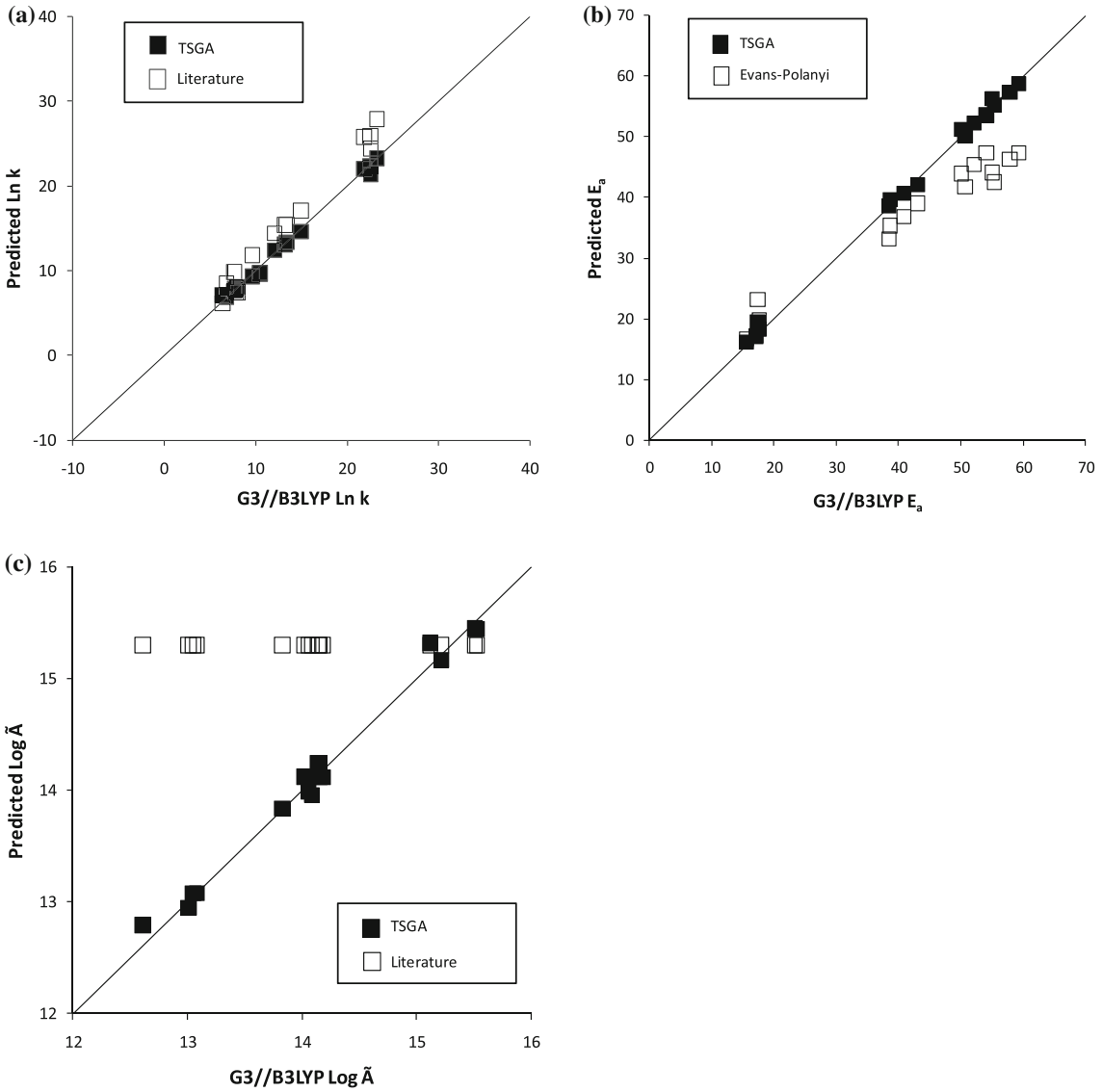

Fig. 12 Parity plots of ring opening for training reactions: **a** ln k at 1,000 K and 1 atm (units for k are s^{-1}), **b** E_a (units for E_a are kcal mol^{-1}), **c** log $\tilde{A}$ (units for $\tilde{A}$ are s^{-1})

rate coefficient for the formation of a three- and four-membered ring by factors of 0.13 and 6.0, respectively, at 1,000 K. Larger cyclic species with two adjacent tertiary silicon atoms (e.g., reaction 21) that sterically hinder the reactive center are captured less well by TSGA; the rate coefficient for cyclization is overpredicted by a factor of 8.8.

The predictions of TSGA were compared to those of the literature correlations for the reactions comprising the validation set. Parity plots of the rate coefficients at 1,000 K and 1 atm, E_a, and log $\tilde{A}$ for both TSGA and the literature correlations are provided in Figs. 13a–c and 14a–c for cyclization and ring opening reactions, respectively. The sum of squared errors between the rate coefficients predicted by TSGA and the G3//B3LYP values is lower than that for the literature correlations which are generalized from silylene addition and elimination reactions. However, the superiority of TSGA is even more clearly demonstrated when the log $\tilde{A}$ and E_a values are examined individually. For the validation set reactions, the mean absolute deviation values for the prediction of G3//B3LYP values with the TSGA method for E_a and log $\tilde{A}$ are 1.20 and 1.84 kcal mol^{-1} and 0.10 and 0.30 for the ring opening and cyclization reactions, respectively. Thus, the predictive capability of TSGA over a wide range of log $\tilde{A}$ and E_a is preferred in the calculation of rate coefficients for the cyclization and ring opening reactions.

Lastly, in the context of ring statistics for hydrogenated amorphous silicon nanostructures, the data for equilibrium concentration distributions based on ring size for the formation of monocyclic species (Fig. 10) have the potential

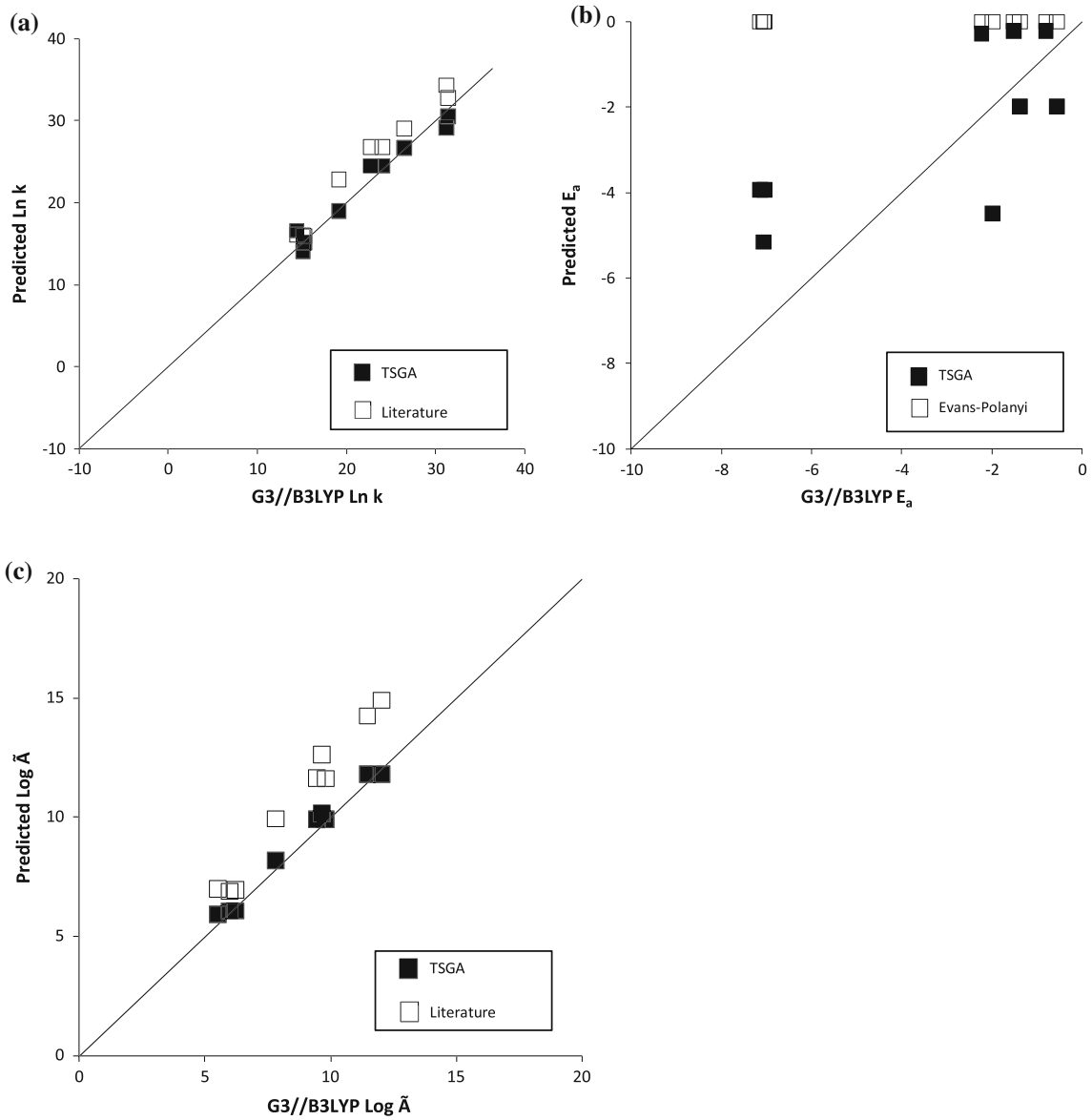

Fig. 13 Parity plots of cyclization for validation reactions: **a** ln k at 1,000 K and 1 atm (units for k are s^{-1}), **b** E_a (units for E_a are kcal mol^{-1}), **c** log $\tilde{A}$ (units for $\tilde{A}$ are s^{-1})

to be extended to polycyclic species formation. Over the temperature range of 750–1,200 K, equilibrium coefficients for reaction 25 calculated from the forward and reverse rate coefficients using the TSGA method have been shown to be within a factor of four of G3//B3LYP equilibrium coefficients.

4 Conclusions

Rate coefficients and Arrhenius parameters for 25 cyclization/ring opening reactions have been calculated using G3//B3LYP, statistical thermodynamics, conventional TST and one-dimensional variational TST and internal rotation corrections. The overall cyclization reaction was found to pass through a stable cyclic intermediate that is enthalpically downhill from the acyclic substituted silylene and that transforms via an exothermic reaction to form a ring for all silicon hydrides. The two elementary steps were investigated separately. The rate-determining step was determined to be from the intermediate species to the ring for three-membered ring formation reactions, and, for four-, five- and six-membered ring formation reactions, the rate-determining step was determined to be from the substituted silylene to the intermediate. Kinetic parameters for the overall reaction assuming a rate-determining step were calculated to align better with mechanistic modeling efforts. The rate coefficients have established a missing

Table 7 Ratio of k^{TSGA} and $k^{G3//B3LYP}$ of the training set for cyclization reactions using the full parameter model

Reaction	Temperature (K)		
	750	1,000	1,200
1	1.00	1.00	1.00
2	1.08	1.48	1.74
3	0.24	0.31	0.35
4	0.24	0.32	0.37
5	0.87	1.05	1.15
6	1.04	1.05	1.05
7	1.44	1.26	1.18
8	0.77	0.72	0.70
9	1.14	1.35	1.46
10	0.97	0.92	0.90
11	1.36	1.34	1.32
12	0.66	0.60	0.57
13	0.06	0.10	0.13
14	0.92	0.70	0.61
15	2.16	1.94	1.83
16	8.14	7.14	6.69

Table 8 Ratio of k^{TSGA} and $k^{G3//B3LYP}$ of the training set for ring opening reactions using the full parameter model

Reaction	Temperature (K)		
	750	1,000	1,200
1	1.00	1.00	1.00
2	0.62	0.74	0.81
3	0.64	0.76	0.83
4	0.39	0.47	0.52
5	1.05	1.16	1.21
6	0.91	0.94	0.95
7	1.06	0.97	0.93
8	0.98	0.95	0.94
9	0.72	0.79	0.83
10	1.03	1.00	0.99
11	1.19	1.20	1.21
12	1.14	1.05	1.01
13	0.20	0.29	0.35
14	1.72	1.44	1.32
15	1.23	1.12	1.08
16	2.32	2.11	2.01

mechanistic connection between acyclic and cyclic silane species on the path to hydrogenated amorphous silicon nanostructure formation. Moreover, the underlying thermodynamic properties for the cyclization and ring opening reactions investigated offer clear evidence that

Table 9 Ratio of k^{TSGA} and $k^{G3//B3LYP}$ of the validation set for cyclization reactions using the full parameter model

Reaction	Temperature (K)		
	750	1,000	1,200
17	0.07	0.13	0.16
18	0.83	0.91	0.96
19	1.87	1.69	1.60
20	7.59	5.98	5.30
21	13.34	8.76	7.10
22	0.65	0.90	1.06
23	0.29	0.36	0.41
24	0.93	1.28	1.51
25	0.25	0.43	0.56

Table 10 Ratio of k^{TSGA} and $k^{G3//B3LYP}$ of the validation set for ring opening reactions using the full parameter model

Reaction	Temperature (K)		
	750	1,000	1,200
17	0.26	0.34	0.39
18	1.35	1.39	1.42
19	1.33	1.18	1.11
20	1.13	1.10	1.08
21	1.56	1.36	1.27
22	0.34	0.51	0.64
23	0.75	0.81	0.84
24	0.75	0.79	0.81
25	0.05	0.10	0.14

hydrogenated amorphous silicon nanostructures will be primarily composed of three-, four- and five-membered rings under pyrolysis conditions.

A group additivity model has been extended to single-event pre-exponential factors, $\tilde{A}$, and activation energies, E_a, for the cyclization and ring opening reactions of silicon hydrides. The cyclization and ring opening reactions were explored for rings containing three to six silicon atoms, polycyclic silicon hydrides, and silicon hydrides containing up to eight silicon atoms. The structural moieties around the reactive center that have the most dominant influence on the kinetic parameters were identified. The presence of internal rotations in the substituted silylene was found to have the strongest influence on the kinetic parameters for cyclization reactions. The TSGA method outperforms the methods in the literature that are currently used to estimate Arrhenius parameters for this class of reactions. The mean absolute ratio of predicted rate coefficients for a validation set of nine reactions was lower for TSGA than for current

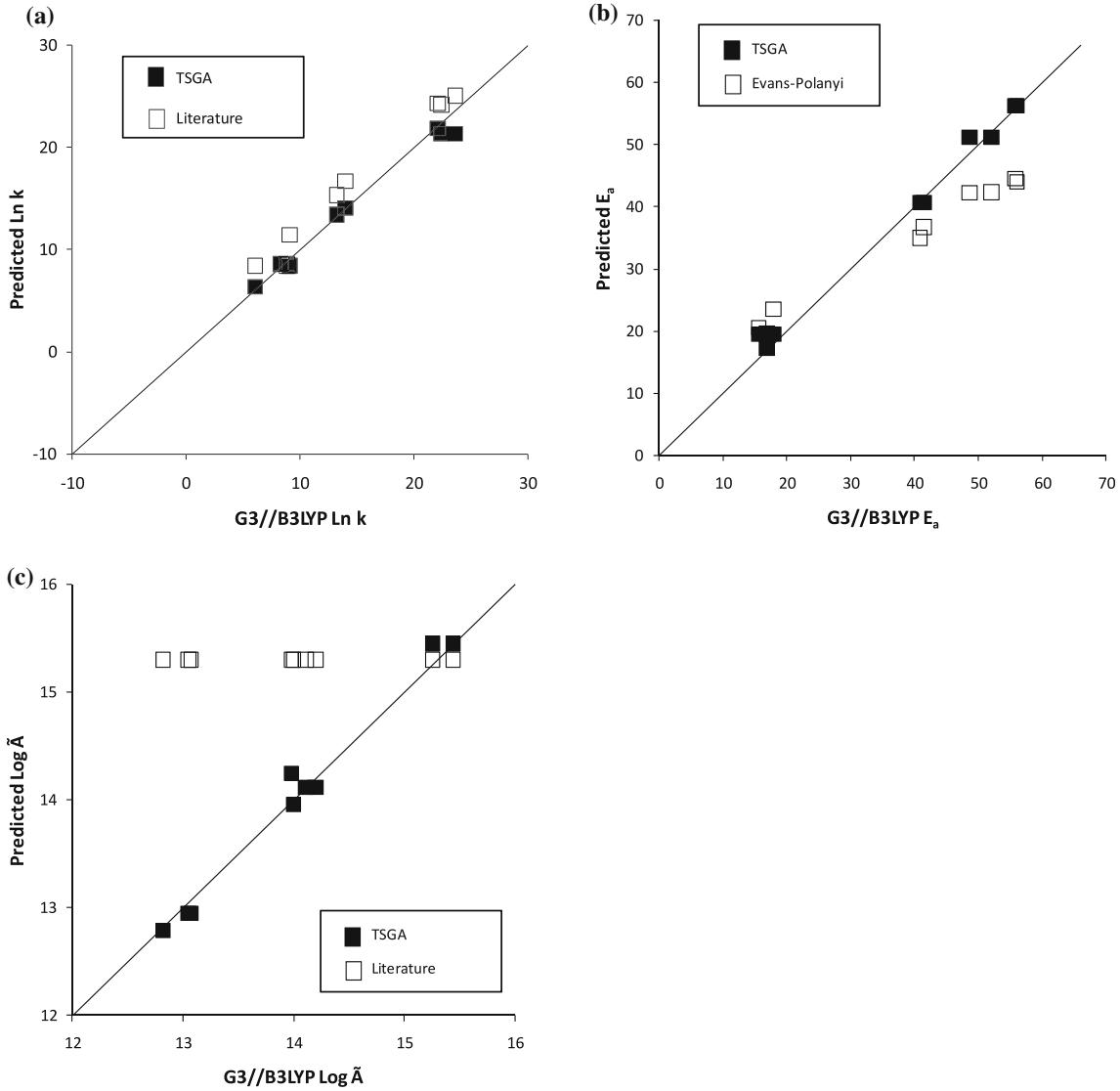

Fig. 14 Parity plots of ring opening for validation reactions: **a** ln k at 1,000 K and 1 atm (units for k are s^{-1}), **b** E_a (units for E_a are kcal mol^{-1}), **c** log $\tilde{A}$ (units for $\tilde{A}$ are s^{-1})

literature methods to predict rate coefficients for cyclization and ring opening reactions.

Acknowledgments We are grateful for the support of this work by the following organizations: (1) National Science Foundation [(a) Collaborative Research Grant CBET-0500320: International Research and Education in Engineering; (b) NCSA Teragrid Supercomputing Facilities], (2) Laboratory for Chemical Technology at Ghent University in Belgium by way of an international fellowship to Andrew J. Adamczyk, and (3) the ARCS Foundation Inc for fellowship support of Andrew J. Adamczyk.

References

1. Swihart MT, Girshick SL (1999) J Phys Chem B 103:64–76
2. Wong HW, Li X, Swihart MT, Broadbelt LJ (2004) J Phys Chem A 108:10122–10132
3. Geng H (2005) Semiconductor manufacturing handbook. McGraw-Hill, USA
4. Teo BK, Sun XH (2007) Chem Rev 107:1454–1532
5. O'Farrell N, Houlton A, Horrocks BR (2006) Int J Nanomed 1:451–472
6. Stueger H, Fuerpass G, Renger K, Baumgartner J (2005) Organometallics 24:6374–6381
7. Morisaki Y, Otaka H, Nagai A, Naka K, Chujo Y (2009) Chem Lett 38:498–499
8. Shimoda T, Matsuki Y, Furusawa M, Aoki T, Yudasaka I, Tanaka H, Iwasawa H, Wang DH, Miyasaka M, Takeuchi Y (2006) Nature 440:783–786
9. Rosenberg L (2006) Nature 440:749–750
10. Hengge E, Janoschek R (1995) Chem Rev 95:1495–1526
11. Hengge E, Bauer G (1975) Monatshefte Fur Chemie 106:503–512
12. Hengge E, Kovar D (1979) Zeitschrift Fur Anorganische Und Allgemeine Chemie 459:123–130
13. Kipping FS, James ES (1921) J Chem Soc 119:830

14. Masamune S, Hanzawa Y, Murakami S, Bally T, Blount JF (1982) J Am Chem Soc 104:1150–1153
15. West R, Indriksons A (1972) J Am Chem Soc 94:6110–6115
16. Carlson CW, West R (1983) Organometallics 2:1801–1807
17. Cypryk M, Gupta Y, Matyjaszewski K (1991) J Am Chem Soc 113:1046–1047
18. Ishikawa M, Kumada M (1972) J Organomet Chem 42:325–332
19. Watanabe H, Shimoyama H, Muraoka T, Kougo Y, Kato M, Nagai Y (1987) Bull Chem Soc Jpn 60:769–770
20. Belzner J (1992) J Organomet Chem 430:C51–C55
21. Suzuki M, Kotani J, Gyobu S, Kaneko T, Saegusa T (1994) Macromolecules 27:2360–2363
22. Ge YB, Head JD (2002) J Phys Chem B 106:6997–7004
23. Blinka TA, West R (1986) Organometallics 5:133–139
24. Sax AF (1986) Chem Phys Lett 129:66–70
25. Sax AF (1986) Chem Phys Lett 127:163–168
26. Schoeller WW, Dabisch T (1987) Inorg Chem 26:1081–1086
27. Mastryukov VS (1992) Izvestiya Vysshikh Uchebnykh Zavedenii Khimiya I Khimicheskaya Tekhnologiya 35:94–97
28. Leong MK, Mastryukov VS, Boggs JE (1994) J Phys Chem 98:6961–6966
29. Zhao M, Gimarc BM (1996) Inorg Chem 35:5378–5386
30. Mastryukov VS, Hofmann M, Schaefer HF (1999) J Phys Chem A 103:5581–5584
31. Swihart MT, Girshick SL (1999) Chem Phys Lett 307:527–532
32. Tang MS, Wang CZ, Lu WC, Ho KM (2006) Phys Rev B 74
33. Singh R (2008) J Phys Condensed Matter 20
34. Ge YB, Head JD (2004) J Phys Chem B 108:6025–6034
35. Balamurugan D, Prasad R (2001) Phys Rev B 64
36. Galashev AE, Izmodenov IA (2008) Glass Phys Chem 34:173–181
37. Li XJ, Li CP, Yang JC, Jalbout AF (2009) Int J Quantum Chem 109:1283–1301
38. Li CP, Li XJ, Yang JC (2006) J Phys Chem A 110:12026–12034
39. Yang JC, Bai X, Li CP, Xu WG (2005) J Phys Chem A 109:5717–5723
40. Li CP, Yang JC, Bai X (2005) Theochem J Mol Struct 755:65–74
41. Xu WG, Yang JC, Xiao WS (2004) J Phys Chem A 108:11345–11353
42. Katzer G, Sax AF (2002) J Phys Chem A 106:7204–7215
43. Katzer G, Ernst MC, Sax AF, Kalcher J (1997) J Phys Chem A 101:3942–3958
44. Sax AF, Kalcher J (1991) J Phys Chem 95:1768–1783
45. Wong HW, Nieto JCA, Swihart MT, Broadbelt LJ (2004) J Phys Chem A 108:874–897
46. Ottosson H, Eklof AM (2008) Coord Chem Rev 252:1287–1314
47. Becerra R, Cannady JP, Dormer G, Walsh R (2009) Phys Chem Chem Phys 11:5331–5344
48. Kusukawa T, Shike A, Ando W (1996) Tetrahedron 52:4995–5005
49. Diez-Gonzalez S, Paugam R, Blanco L (2008) Eur J Organic Chem 19:3298–3307
50. Xu CH, Wakamiya A, Yamaguchi S (2004) Org Lett 6:3707–3710
51. Zhang SG, Liu JH, Zhang WX, Xi ZF (2009) Prog Chem 21:1487–1493
52. Liu JH, Zhang WX, Xi ZF (2009) Chin J Org Chem 29:491–503
53. Trost BM, Bertogg A (2009) Org Lett 11:511–513
54. Guida-Pietrasanta F, Boutevin B (2005) Polysilalkylene or silarylene siloxanes said hybrid silicones. Inorganic polymeric nanocomposites and membranes. Springer, Berlin, pp 1–27
55. Li RE, Sheu JH, Su MD (2007) Inorg Chem 46:9245–9253
56. Segmuller T, Schluter PA, Drees M, Schier A, Nogai S, Mitzel NW, Strassner T, Karsch HH (2006) Dianionic amidinates at silicon and germanium centers: four-, six- and eight-membered rings. In: 11th international symposium on inorganic ring systems (IRIS-11). Elsevier, Finland
57. Broadbelt LJ, Stark SM, Klein MT (1994) Chem Eng Sci 49:4991–5010
58. Broadbelt LJ, Stark SM, Klein MT (1996) Comput Chem Eng 20:113–129
59. Broadbelt LJ, Stark SM, Klein MT (1995) Ind Eng Chem Res 34:2566–2573
60. Broadbelt LJ, Stark SM, Klein MT (1994) Ind Eng Chem Res 33:790–799
61. Klinke DJ, Broadbelt LJ (1997) Aiche J 43:1828–1837
62. Susnow RG, Dean AM, Green WH, Peczak P, Broadbelt LJ (1997) J Phys Chem A 101:3731–3740
63. Broadbelt LJ, Pfaendtner J (2005) Aiche J 51:2112–2121
64. Evans MG, Polanyi M (1938) Faraday Soc 34:11–29
65. Girshick SL, Swihart MT, Suh SM, Mahajan MR, Nijhawan S (2000) J Electrochem Soc 147:2303–2311
66. Ho P, Coltrin ME, Breiland WG (1994) J Phys Chem 98:10138–10147
67. Benson SW (1976) Thermochemical kinetics, 2nd edn. Wiley, New York
68. Sumathi R, Carstensen HH, Green WH (2001) J Phys Chem A 105:6910–6925
69. Sumathi R, Carstensen HH, Green WH (2001) J Phys Chem A 105:8969–8984
70. Sumathi R, Carstensen HH, Green WH (2002) J Phys Chem A 106:5474–5489
71. Saeys M, Reyniers MF, Marin GB, Van Speybroeck V, Waroquier M (2004) Aiche J 50:426–444
72. Saeys M, Reyniers MF, Van Speybroeck V, Waroquier M, Marin GB (2006) ChemPhysChem 7:188–199
73. Sabbe MK, Reyniers MF, Van Speybroeck V, Waroquier M, Marin GB (2008) ChemPhysChem 9:124–140
74. Willems PA, Froment GF (1988) Ind Eng Chem Res 27:1959–1966
75. Willems PA, Froment GF (1988) Ind Eng Chem Res 27:1966–1971
76. Truong TN (2000) J Chem Phys 113:4957–4964
77. Zhang SW, Truong TN (2003) J Phys Chem A 107:1138–1147
78. Baboul AG, Curtiss LA, Redfern PC, Raghavachari K (1999) J Chem Phys 110:7650–7657
79. Katzer G, Sax AF (2005) J Comput Chem 26:1438–1451
80. Katzer G, Sax AF (2003) Chem Phys Lett 368:473–479
81. Ayala PY, Schlegel HB (1998) J Chem Phys 108:2314–2325
82. Pfaendtner J, Yu X, Broadbelt LJ (2007) Theor Chem Acc 118:881–898
83. Van Speybroeck V, Vansteenkiste P, Van Neck D, Waroquier M (2005) Chem Phys Lett 402:479–484
84. Vansteenkiste P, Van Speybroeck V, Marin GB, Waroquier M (2003) J Phys Chem A 107:3139–3145
85. Ashcraft RW, Green WH (2008) J Phys Chem A 112:9144–9152
86. Catoire L, Swihart MT, Gail S, Dagaut P (2003) Int J Chem Kinet 35:453–463
87. Frisch MJ, Trucks GW, Schlegel HB, Scuseria GE, Robb MA, Cheeseman JR, Montgomery JA Jr, Vreven T, Kudin KN, Burant JC, Millam JM, Iyengar SS, Tomasi J, Barone V, Mennucci B, Cossi M, Scalmani G, Rega N, Petersson GA, Nakatsuji H, Hada M, Ehara M, Toyota K, Fukuda R, Hasegawa J, Ishida M, Nakajima T, Honda Y, Kitao O, Nakai H, Klene M, Li X, Knox JE, Hratchian HP, Cross JB, Bakken V, Adamo C, Jaramillo J, Gomperts R, Stratmann RE, Yazyev O, Austin AJ, Cammi R, Pomelli C, Ochterski JW, Ayala PY, Morokuma K, Voth GA, Salvador P, Dannenberg JJ, Zakrzewski VG, Dapprich S, Daniels AD, Strain MC, Farkas O, Malick DK, Rabuck AD, Raghavachari K, Foresman JB, Ortiz JV, Cui Q, Baboul AG, Clifford S, Cioslowski J, Stefanov BB, Liu G, Liashenko A,

Piskorz P, Komaromi I, Martin RL, Fox DJ, Keith T, Al-Laham MA, Peng CY, Nanayakkara A, Challacombe M, Gill PMW, Johnson B, Chen W, Wong MW, Gonzalez C, Pople JA (2004) Gaussian 03, Revision D01. Gaussian, Inc, Wallingford
88. Kalcher J, Sax AF (1992) Theochem J Mol Struct 85:287–302
89. Adamczyk AJ, Reyniers MF, Marin GB, Broadbelt LJ (2010) ChemPhysChem (in press)
90. Scott AP, Radom L (1996) J Phys Chem 100:16502–16513
91. Vansteenkiste VVS P, Verniest G, De Kimpe N, Waroquier M (2006) J Phys Chem A 110:3838–3844
92. Martin JML, de Oliveira G (1999) J Chem Phys 111:1843–1856
93. McQuarrie DA, Simon JD (1999) Molecular thermodynamics. University Science Book, Sausalito
94. Hirschfelder JO, Wigner E (1939) J Chem Phys 7:616–628
95. Fernandez-Ramos A, Ellingson BA, Meana-Paneda R, Marques JMC, Truhlar DG (2007) Theor Chem Acc 118:813–826
96. Truhlar DG, Garrett BC (1984) Annu Rev Phys Chem 35:159–189
97. Truhlar DG, Gordon MS (1990) Science 249:491–498
98. Adamczyk AJ, Reyniers M-F, Marin GB, Broadbelt LJ (2009) J Phys Chem A 113:10933–10946
99. Gupta A, Swihart MT, Wiggers H (2009) Adv Funct Mater 19:696–703
100. Wiggers H, Starke R, Roth P (2001) Chem Eng Technol 24:261–264
101. Becerra R, Frey HM, Mason BP, Walsh R, Gordon MS (1992) J Am Chem Soc 114:2151–2752
102. McCarthy MC, Yu Z, Sari L, Schaefer HF, Thaddeus P (2006) J Chem Phys 124:7
103. Street RA (1991) Hydrogenated amorphous silicon. Cambridge University Press, London
104. Schulke W (1981) Philos Mag B Phys Condens Matter Stat Mech Electronic Optical Magn Prop 43:451–468